JBC Papers in Press. Published on May 16, 2016 as Manuscript M116.727248
The latest version is at http://www.jbc.org/cgi/doi/10.1074/jbc.M116.727248

ACTIVITY OF MENKES DISEASE PROTEIN ATP7A IS ESSENTIAL FOR REDOX BALANCE IN MITOCHONDRIA

Ashima Bhattacharjee[1ʃ*], Haojun Yang[1*], Megan Duffy[2], Emily Robinson[2Ω], Arianrhod Conrad-Antoville[2], Ya-Wen Lu[1], Tony Capps[2], Lelita Braiterman[3], Michael Wolfgang[4], Michael P. Murphy[5], Ling Yi[6], Stephen G. Kaler[6], Svetlana Lutsenko[1¶*], Martina Ralle[2¶*]

[1]Department of Physiology, Johns Hopkins University School of Medicine, Baltimore, MD; [2]Department of Molecular and Medical Genetics, Oregon Health & Science University, Portland, OR; [3]Department of Biological Chemistry and [4]-Department of Cell Biology, Johns Hopkins University School of Medicine; [5]MRC Mitochondrial Biology Unit, Cambridge, United Kingdom, [6]Section on Translational Neuroscience, Eunice Kennedy Shriver National Institute of Child Health and Human Development, National Institutes of Health, Bethesda, MD

Running Title: ATP7A is essential for redox balance in mitochondria

Copper-transporting ATPase ATP7A is essential for mammalian copper homeostasis. Loss of ATP7A activity is associated with fatal Menkes disease (MD) and various other pathologies. In cells, ATP7A inactivation disrupts copper transport from cytosol into the secretory pathway. Using fibroblasts from MD patients and mouse 3T3-L1 cells with a CRISPR/Cas9 inactivated ATP7A, we demonstrate that ATP7A dysfunction is also damaging to mitochondrial redox balance. In these cells, copper accumulates in nuclei, cytosol, and mitochondria, causing distinct changes in their redox environment. Quantitative imaging of live cells using GRX1-roGFP2 and HyPer sensors reveals highest glutathione oxidation and elevation of H_2O_2 in mitochondria, whereas the redox environment of nuclei and cytosol is much less affected. Decreasing the H_2O_2 levels in mitochondria with MitoQ does not prevent glutathione oxidation, i.e. elevated copper, and not H_2O_2 is a primary cause of glutathione oxidation. Redox misbalance does not significantly affect mitochondria morphology or activity of respiratory complex IV but markedly increases cell sensitivity to even mild glutathione depletion, resulting in loss of cell viability. Thus, ATP7A activity protects mitochondria from excessive copper entry, which is deleterious to redox buffers. Mitochondrial redox mis-balance could significantly contribute to pathologies associated with ATP7A inactivation in tissues with paradoxical accumulation of copper (i.e. renal epithelia).

Copper is an essential cofactor for numerous enzymes including Cu/Zn-superoxide dismutase (SOD1), cytochrome c oxidase (COX), tyrosinase, dopamine-β-hydroxylase, lysyl oxidase, and many others. These enzymes are involved in physiological processes that are indispensable for life. Consequently, copper deficiency is deleterious and can result in death (1,2). Copper is transported into cells predominantly by a copper-transporter CTR1; this process is facilitated by intracellular glutathione(3). Excess copper is removed from the cell by the ATP-driven copper transporters (Cu(I)-ATPases) ATP7A and ATP7B. ATP7A is the major regulator of copper homeostasis in most human cells. ATP7A uses energy of ATP hydrolysis to transfer copper from the cytosol into the lumen of secretory pathway for functional maturation of copper-dependent enzymes within this compartment. ATP7A also sequesters excess copper in vesicles, which eventually fuse with the plasma membrane allowing copper export. Inactivation of ATP7A results in a fatal Menkes disease (1,2). ATP7A mutations have also been linked to Occipital Horn Syndrome (OHS) and isolated distal motor neuropathy (4). In these allelic variants, mutant ATP7A retains some function and the diseases

¶ To whom correspondence should be addressed: Svetlana Lutsenko, 725 N. Wolfe street, Baltimore, MD, 21205; Lutsenko@jhmi.edu and Martina Ralle, 3181 SW Sam Jackson Park Rd, Portland, OR, 97239, rallem@ohsu.edu
Present affiliations - [ʃ]S.N.Pradhan Center for Neurosciences, University of Calcutta, Kolkata, India [Ω]AbSci, LLC, Portland, OR; [ƒ]Department of Neuroscience, Johns Hopkins University School of Medicine, Baltimore, MD
* equal contributions

have a milder course with better survival. Several inbred mouse strains with mutations in ATP7A exist and has been used to explore consequences of ATP7A inactivation (5-7). Recently, a targeted deletion of ATP7A in motor neurons in mice was shown to trigger age-dependent muscle atrophy resembling the phenotype of human X-linked spinal muscular atrophy type 3. In this later case, the role of ATP7A in systemic copper homeostasis was unaltered and pathology reflected the loss of important ATP7A functions in motor neurons (8)

The functional significance of ATP7A at the level of whole organism is firmly established: ATP7A facilitates export of copper from the intestine and mediates copper entry into the brain (9). ATP7A inactivation results in systemic copper deficiency, especially in the central nervous system (CNS). In brains of Menkes disease (MD) patients, activity of Cu-dependent enzymes is decreased and changes in myelination, energy metabolism, catecholamine balance, and mRNA translation are evident (10). However, in MD not all tissues are copper deficient. Certain organs and tissues, e.g., kidney and intestine, accumulate copper (11-13). In such peripheral tissues mechanisms of pathology caused by ATP7A inactivation may not be identical to those in the CNS (4-7). Copper supplementation therapy, commonly used to improve conditions in MD may exacerbate the copper-accumulating tendency in such tissues and have a negative impact (13,14).

Currently, the information about cellular consequences of ATP7A inactivation is limited. Studies using patient skin fibroblasts have shown that the loss of ATP7A function results in elevation of cellular copper content (4,5) and upregulation of proteins involved in copper sequestration (metallothioneins) and DNA repair (15). It remains unclear whether Cu acts primarily in the nuclei or detected changes in the mRNA profiles are caused by metabolic changes in other compartments and/or inter-compartment signaling (6). It was proposed that mitochondria contribute to the maintenance of cellular copper balance by communicating changes in its metabolic status to ATP7A (16). Whether and how inactivation of ATP7A alters functions of mitochondria or any other cell compartment, beyond the secretory pathway, is unclear. In this study, we have systematically addressed this issue.

We have found that in ATP7A$^{-/-}$ cells (human skin fibroblasts as well as mouse pre-adipocytes), copper is elevated in several intracellular compartments and has distinct effects on their redox environment. Mitochondria are most impacted and show an increased oxidation of glutathione and thioredoxin (the two major redox buffers) as well as accumulation of peroxide. Although cell growth is not inhibited, ATP7A$^{-/-}$ cells are highly sensitive to a decrease of total glutathione content. These results highlight a previously unanticipated consequence of ATP7A dysfunction for mitochondrial redox homeostasis and suggest that abnormal mitochondrial redox status may contribute significantly to MD pathogenesis in peripheral tissues and to pathologies associated with a cell-specific loss of ATP7A function. Cells and tissues with a low glutathione content and/or high demand for mitochondria function may be especially at risk.

EXPERIMENTAL PROCEDURES

Cell culture and fractionation. Generation of immortalized skin fibroblast from the MD patient (YS cells) and the mother of this patient (XS cells) were previously described (17)). The mutation in ATP7A in YS cells, a single base-pair deletion of Cytidine1638 in exon 6th, was identified using exon amplification and direct sequencing of the PCR products. A detected deletion of a base pair in the nucleotide C1638 in the patient ATP7A transcript is predicted to produce a frameshift at the amino acid position 546 followed by eight unrelated amino acids. XS cells showed the same PCR product, but uniformly lacked the mutation, i.e. genotype of control cells was *ATP7A*$^{+/+}$. The lack of mutation is due to a mosaic nature of carrier' skin, which permits isolation of cells with both normal alleles. Additional control cell line GM3440 included cultured fibroblasts from an unrelated healthy. Two MD fibroblasts cell line (MF1, and MF2 cells) derived from a patient with mutation Q724H (18) and IVS8 AS dup5 mutation (19), respectively. The *ATP7A*$^{-/-}$ *3T3-L1* cells were generated as described below using mouse 3T3-L1 cells (ATCC) and the CRSPR/Cas9 protocol.

The fibroblasts, HEK293T and 3T3-L1 cells were cultured in DMEM (Gibco) supplemented with 10% FBS (Sigma Aldrich) and 1% Penstrep (Gibco). For sub cellular fractionation experiments, cells grown on 15cm dishes were washed with Phosphate Buffered Saline (PBS), trypsinized and washed with PBS. Cell pellets are resuspended with 1ml of lysis buffer (PBS containing 1mM EDTA, 1mM EGTA, 1mM 4-(2-Aminoethyl) benzenesulfonyl fluoride hydrochloride, 0.1 volume of 2.5M sucrose and protease inhibitor cocktail (Roche)), homogenized with a loose pestle dounce homogenizer (100 strokes) and 220 strokes with a tight pestle (step1). The homogenate was centrifuged at 600xg for 6 minutes. The pellet was washed twice in PSE buffer (PBS containing 1mM EDTA, 300mM sucrose, 0.1% IGEPAL and complete protease inhibitor cocktail (Roche)). The pellet was resuspended in PSE buffer containing 0.2% Triton-X and used as a nuclei-enriched fraction. The supernatant from step 1 was centrifuged at 10,000Xg for 10 minutes to pellet mitochondria. The pellet was resuspended in PSE buffer containing 0.2% Triton-X. The supernatant was kept as a post mitochondria fraction (cytosol). Mitochondria purity was examined by Western blotting (n=3) and densitometry using lamin and TIM23 as markers of nuclei and mitochondria, respectively. The nuclear contamination of mitochondria fraction was 24%.

Copper content in cells and cell fractions. Cells were transferred to a pre-cleaned polypropylene tube, pelleted by centrifugation and the resulting pellets washed with ice-cold PBS. Cell pellets and cell fractions were digested in 50% HNO_3 (trace metal grade, Fisher Scientific, Fair Lawn, NJ) by incubating at 90°C for 3 hrs. Upon completion, an equal amount of hydrogen peroxide (trace metal grade, Fisher Scientific, Fair Lawn, NJ) was added and the resulting solution diluted with 1% HNO_3 to achieve a final concentration of HNO_3 below 5%. ICP-MS (Inductively Coupled Plasma Mass Spectrometry) analysis was performed using an Agilent 7700x equipped with an ASX 500 autosampler. The system was operated at a radio frequency power of 1550 W, an argon plasma gas flow rate of 15 l/min, Ar carrier gas flow rate of 1.04 l/min. Elements were measured in kinetic energy discrimination (KED) mode using He gas (4.3 ml/min). Data were quantified using a 10-point calibration curve (0.5-5000 ppb (ng/g) range) with external standards for Ca, Mn, Fe, Cu, Zn (elemental mix 2, VHG Labs, Manchester, NH) in inorganic diluent (1% HNO_3) to match the sample matrix. For each sample, data were acquired in triplicate and averaged. Internal standards (^{45}Sc, ^{72}Ge, and ^{209}Bi) were introduced with the sample to correct for plasma instabilities; a 10 ppb standard solution containing Ca, Mn, Fe, Cu, and Zn, and a blank containing diluent only were used to calculate the coefficient of variance (CoV). To ensure maximum recovery of elements, certified NIST (Gaithersburg, MD) standard reference material (bovine liver, SRM 1577c) was treated and prepared by the same method as the samples and analyzed. To determine background concentrations from materials used in the analysis, a blank tube was treated as a sample and elemental contents measured. All glass and plastic ware used in ICP-MS analysis were rinsed with and/or stored in 1% HNO_3 until use. To quantify concentration of elements in cells, diameters of trypsinized cells (that have spherical shape) were determined using the automated features of a Biorad cell counter (TC10, Biorad, Herkules, Ca), averaged and cell volumes were calculated.

The copper content of control, MF1, MF2 and $ATP7A^{-/-}$ 3T3-L1 cells was determined using a Shimadzu 6650 graphite furnace atomic absorption spectrophotometer equipped with an ASC-6100 autosampler. Cell pellets were dissolved with HNO_3, and heated at 50^0C for 30 min. Samples were diluted with double distilled H_2O to be in the linear absorption range of the calibration curve (1–10 ppb). Each sample was measured 2-3 times, and the concentration of copper was derived from the calibration curve. Protein concentration or initial cell number was used for normalization. Experiments were repeated three times with three technical replicates.

X-ray fluorescence microscopy (XFM). For XFM experiments, cells were grown onto 4 x 4 mm silicon nitride membranes (SiN, Silson Ltd, North Hampton, England). SiN membranes were sterilized with UV radiation and incubated with 10 µL sterile 0.01% POLY-L-Lysine solution (Sigma-Aldrich, St Louis, MO) at 37ºC. After 30 min, POLY-L-Lysine was removed and 10 µl of

cell containing media was added to the membrane. Basal medium was added to the cultures after 15 min at 37ºC. After completion of the experiments the membranes were rinsed with PBS, fixed with 2% paraformaldehyde for 30 min at 37ºC, rinsed with PBS, isotonic 100 mM ammonium acetate, DI water and air-dried. XFM data were collected on beamline 2-ID-E at the Advanced Photon Source, Argonne National Laboratory, Argonne, IL. SiN membranes were mounted onto kinematic sample holders and target cells were selected using a light microscope (Leica, Buffolo Grove, IL) equipped with a high precision, motorized x, y-stage (Ludl Electronic Products, Hawthorne, NY). Coordinates of target cells were recorded before mounting the sample on the microprobe stage at the beamline. The microscope coordinates were translated into microprobe coordinates and the cell raster scanned in the x-y plane. The incident X-ray energy was tuned to 10 keV using a Si-monochromator, the monochromatic beam was focused to 750 x 750 nm using a Fresnel zone plate. The sample was placed at 19º to the incident X-ray beam and the resulting X-ray fluorescence was collected at 90º using an energy dispersive 4-element detector (Vortex ME-4, SII Nanotechnology, Northridge, CA). Elemental maps were created by extracting, background subtracting, and fitting the fluorescence counts for each element at each point using the program MAPS (20). The fluorescent photon counts were translated into μg/cm^2 using calibrated X-ray standards (AXO products, Dresden, Germany).

Generation of NLS-GRX1-roGFP2 and MTS-GRX1-roGFP2. To target sensor to the nucleus, the 'SPKKKRKVE' Nuclear Localization Signal (NLS) from SV40 and a linker sequence (Ser-Gly)$^{4+4}$ were added at to the N-terminus of GRX1-roGFP2 (21). The DNA sequence: 5'-AGCCCGAAGAAAAAACGTAAAGTGGAG-3' encoding the NLS and the 5'-AGCGGGAGC-GGGAGCGGGAGCGGG-3' sequence encoding the linker were inserted at the 5' end of GRX1-roGFP2 cDNA using overlapping PCR. The insert was cloned into pEIGW vector using SmaI and EcoRI restriction sites at 5' and 3' end respectively. To target a sensor to mitochondria (MTS-GRX1-roGFP2), three mitochondria targeting sequences (MTS) MSVLTPLLLRGL-TGSARR were inserted in tandem at the N-terminus of GRX1-roGFP2. This was done by inserting 3 copies of 5' ATGTCCGTCCTGACG-CCGCTGCTGCTGCGGGGCTTGACAGGCTCG GCCCGGCGG 3' sequence at the 5' end of GRX1-roGFP2 cDNA using overlapping PCR.

Live cell imaging. To evaluate the GSH:GSSG ratio, the YS and control cells were plated on FD-35 Fluorodishes and transiently transfected with 1000 ng of GRX1-roGFP2, NNLS-GRX1-roGFP2 or MTS-GRX1-roGFP2 using Lipofectamine LTX PLUS (Life Technologies) following manufacturer's protocol. Cells were cultured overnight in DMEM without phenol red (Gibco) and then imaged with Zeiss LSM510 Meta and Zeiss LSM700 confocal laser scanning microscope. The sensor was excited frame by frame with 405 and 488 nm laser and emission detected using 500-554 band pass filter. To verify responsiveness of the GRX1-roGFP2 sensors to oxidation/reduction, HEK293T cells transiently expressing the sensors were imaged under basal condition and in response to treatment with 100 μM H_2O_2 and 500μM DTT. Images showing ratio of fluorescence intensities after exciting at two wavelengths ($IR_{405/488}$) were prepared using Zen2009 software after subtracting background. To measure levels of peroxide YS, control and HEK293T were transiently transfected with the HyPer sensor targeted to nucleus, mitochondria or cytosol (22). Intensity Ratio ($IR_{488/405}$) images were also prepared using Zen2009 software after subtracting background.

Analysis of glutathione in cell lysates and fractions. All reactions and dilutions unless mentioned otherwise were conducted in 10 mM sodium phosphate, 1 mM EDTA, pH 7.2; 400 μl of 5% 5-sulfosalicylic acid (SSA) was added to each cell pellet (~1,6 w/v dilution) to lyse cells and deproteinize cell contents. The lysis product was stored -80 °C until use, spun down; the supernatant was used to determine soluble GSH. The deproteinization step was avoided in estimation of GSH in organelle extracts. For copper chelation, the mitochondria-enriched fraction was incubated with 50 or 100uM BCS on ice for 3 hours. Glutathione content was determined by a modified version of the colorimetric recycling assay using 5,5'-dithiobis(2-nitrobenzoic acid, DTNB (23). Absorbance of the

reaction product was monitored at 412 nm for up to 40 cycles using a microplate reader (FLUOstar Omega, BMG Labtech). The slope was determined using the linear range of the curve and compared to that of a standard curve for known GSH concentrations. All samples were assayed in triplicate and results corrected from the total cell count and volume for a given sample.

Rescue of mitochondria glutathione balance by restoration of copper export. Several attempts to generate human Cherry-ATP7A were unsuccessful due to rearrangements within the cDNA sequence. Consequently, to restore copper transport within the secretory pathway a homologous ATP7B was used. YS cells were cultured on fluorodishes and transiently cotransfected with Cherry-ATP7B and MTS-GRX1-roGFP2 plasmids (1000ng each) following protocol described above. Cells co expressing proteins and those expressing only MTS-GRX1-roGFP2 were selected for comparison from the same culture dish.

Electron Microscopy. MF1, MF2 and control GM3440 cells were fixed in 2% gluteraldehyde, 2% paraformaldehyde, 0.1 M sodium cacodylate, 3 mM $MgCl_2$, pH 7.2 for 1 h at room temperature. After buffer rinse, the samples were incubated for 1.5 h in 1% osmium tetroxide in 0.1 M sodium cacodylate, 3 mM $MgCl_2$ on ice in the dark. Following wash with 50 mM Maleic acid, 3% sucrose, pH to 6.2, samples were stained with 2% uranyl acetate for 1 h at room temperature in the dark. Samples dehydrated in a graded series of ethanol and embedded in Eponate 12 (Ted Pella) resin. Samples were polymerized at 37°C for 2-3 days before moving to 60C overnight. Thin sections, 60 to 90 nm, were cut with a diamond knife on the Reichert-Jung Ultracut E ultramicrotome and picked up with 2x1 mm formvar coated copper slot grids and grids were stained with 2% uranyl acetate in 50% methanol and 0.4% lead citrate before (prepared by JHU School of Medicine MicFac). The sections were then examined on a Hitachi 7600 TEM at 80 kV. Images were captured with an AMT XR50 CCD (5 megapixel) camera.

Cytochrome c oxidase activity. YS and control cells were grown on six 15cm dishes to 80-90% confluency. Cell pellets are resuspended in IBc (10mM Tris, EGTA and 200mM sucrose) buffer, homogenized with 45 strokes in precooled small Teflon dounce at 1600rpm. The homogenate was centrifuged twice at 600g for 10 min at 4^0C. The supernatant was collected and centrifuged at 7000g for 10 min at 4^0C. The pellet was washed by resuspending in IBc buffer and centrifuging at 7000g at 4^0C. The pellet was resuspended in IBc buffer and centrifuged at 10,000g for 10 min at 4^0C and resuspended in 250mM mannitol, 5mM HEPES pH 7.4, and 0.5mM EGTA.

Activity of Complex IV was measured by following the initial rate of ferro-cytochrome c oxidation at 550nm using a protocol adapted from (7). Briefly, equine cytochorme c at 0.8% (weight per reaction volume of 50mM potassium phosphate, 2mM EDTA, pH7.4 reaction buffer) was reduced with 1M DTT (0.1 μl per 80 ml of solution) for 20 minutes at room temperature. The cytochrome c solution was then concentrated using Amicon Ultra 0.5ml 10K cutoff filters (Millipore), diluted with buffer to the final concentration is 0.08% (w/v) and then 1,10 with water to reach OD=1.8-1.9. The reaction was initiated by the addition of 30 μg of mitochondria fraction solubilized with 0.5% n-dodecyl b-D-maltoside (Anatrace) at a final concentration of 5 mg/ml in reaction buffer supplemented with 1mM PMSF, 10uM leupeptin, and 2uM pepstatin A, and the change in absorbance followed for 150 seconds. Each sample was measured thrice and the data averaged. The extinction coefficient for reduced cytochrome c used for calculating the rate of oxidation expressed as a change cytochrome absorption per minute divided e_{550} x mg mitochondria, where e_{550}=19.6mmolxL^{-1}xcm^{-1}.

Oxidation state of thioredoxin (Trx1) Differentially oxidized forms of Trx1 were characterized as previously described (24,25). Briefly, cells grown in basal medium were harvested, resuspended in a buffer containing 6 M guanidine, 50 mM Tris-HCl, pH 8.3, 3 mM EDTA, and sonicated for 4 sec four times followed by centrifugation at 1000 x g and incubated with 5.5 μM iodoacetic acid (IAA) at 37ºC for 30 min to carboxymethylate Trx1. To generate fully reduced and oxidized samples, samples were treated for 30 minutes with either 40 mM DTT or 5 mM H_2O_2, respectively, prior to

IAA incubation. Gel-electrophoresis was performed using a 12% native pre-cast polyacrylamide gel and native tris-glycine buffer at 225 V on ice. Proteins were transferred to a PDVF membrane and probed using rabbit-α-Trx1 antibody (1 :500, in 5 % milk TBST, overnight at 4ºC; Santa Cruz Biotechnology) and horseradish peroxidase-conjugated goat-α-rabbit secondary antibody (1:10,000 in 5% milk TBST, 1.5 hrs; ABCAM) followed by chemiluminescent detection with ECL Western blotting substrate (Pierce, Thermo Scientific) using a FlourChem E system (Protein Simple).

Generation of 3T3-L1-ATP7A$^{-/-}$ cells using Cas9-CRISPR system.
Human codon-optimized Cas9 expression vector was obtained from Addgene, plasmid #41815 (26), and Cas9 was cloned into a pEF6 expression vector, downstream and in-frame with a nuclear-localized YFP, linked by a viral 2A bicistronic peptide (27), such that nls-YFP and Cas9 are expressed in approximate equimolar quantities. A guide RNA (gRNA), including the U6 promoter, was synthesized as a 500bp gBlocks fragment (Integrated DNA Technologies) and was cloned into the pEF6-nls-YFP-2A-Cas9 vector by InFusion Cloning (Clontech). The sgRNA sequences were designed to target trans-membrane regions of ATP7A gene and determined by the CRISPR Design Tool (http,//crispr.mit.edu/). Two synthesized sgRNA oligos (Integrated DNA Technology) for each gene (ATP7A target 1: GTTTTTCTGTATCCCTGTAATGG and ATP7A target 2: CCTATGCTGTTTGTGTTTATTGC) were ligated into Cas9 vector using In-Fusion HD Cloning Kit (Clontech Laboratories). Undiferentiated 3T3-L1 Cells were transfected with the resulting plasmid using Lipofectamine LTX with Plus Reagent (Life Technologies). Transfected cells were selected by 3ug/ml blasticidin in cell culture medium for two weeks, then diluted into 96-well plate for cell cloning. The clones were expanded into larger plates till cell number exceeded 1 x 10^6 and the cryo-stocks were prepared. The 3T3-L1-ATP7A$^{-/-}$ cells were identified by Western blotting analysis of cell homogenates. Briefly, cells were collected from 10 cm dish and homogenized in 25mM Imidazole, pH7.4, 0.25M sucrose, 2mM AEBSF, one tablet of EDTA-free protease inhibitor cocktail. The protein concentration was estimated using BCA assay. 20 µg of homogenate was separated on 7.5% polyacrylamide gels, then transferred onto polyvinyldifluoride (PVDF) membrane and incubated overnight at 4^{o}C with rabbit anti-ATP7A CT77 (Hycult Biotech) to detect ATP7A and with mouse anti-tubulin (Sigma), used as a loading control. Deletions in the ATP7A gene were identified by Sanger sequencing. Specifically, genomic DNA from positive cell clones was isolated using GenElute Mammalian Genomic DNA miniprep Kit (Sigma-Aldrich) and the targeted region of ATP7A gene was amplified by PCR using forward primer: 5'-TCTTAGCCTGAGTGAGATGGTT-3' and reverse primer: 5'-TCCACTATCTTAACAA-ATGTCACCC-3'. PCR products were cloned into the TOPO vector using TOPO TA cloning Kit (Life Technologies) and transformed into Top 10 competent cells (Life Technologies). Plasmids were then isolated using QIAprep Spin Miniprep Kit (Qiagen) for Sanger sequencing.

Redox Imaging. Control, MF1, MF2 and 3T3-L1-ATP7A$^{-/-}$ cells transiently expressing MTS-GRX1-roGFP2 were grown in 35 mm dishes and treated with 200 µM H_2O_2 or 1 mM DTT to achieve complete sensor oxidation and reduction respectively. Ratiometric ($IR_{405/488}$) images were prepared using Image J software after subtracting background. $IR_{405/488}$ images were then converted to percentage oxidation of MTS-GRX-roGFP2 using Hanson's equation.

Real-Time PCR. To compare levels of IFI27 mRNA, YS and control cells were cultured in 6 cm tissue culture dishes were treated with either 0 or 50nM MitoQ for 24 hours. For relative quantitation of Metallothionein 1 (MT1) mRNA, YS and control cells were cultured under basal condition. Cells were then harvested, washed with PBS, lysed using QIAshredder (Qiagen) and RNA extracted with RNeasy minikit (Qiagen). The cDNA was prepared by reverse transcription using Transcriptor First Strand cDNA synthesis kit (Roche Applied Science) using 1 µg of RNA in a final volume of 20 µl using both anchored oligo(dT)18 and random hexamer primer following manufacturer's instructions. Real-time PCR was performed using 1 µl of the prepared cDNA in a 20-µl reaction volume with Power

SYBR Green PCR Master Mix (Applied Biosystems). Levels of IFI27 transcript were estimated using primers against a region of cDNA common for IFI27 isoforms. Forward primer 5' CTCAGGAACTCTCCTTCTTTGG 3' (exon 3) and reverse primer 5' CCTGCTCGGGTTA-ATTCCGTGG 3' were used. Amount of MT1 transcript was estimated using forward primer 5' CCTGTGCCAGCTCCTGCAAGTGC 3' and reverse primer 5' CCAGGTTTGTGCAGG-TTGCTCTG 3'. Beta actin mRNAwas used as a reference. The PCR involved initial denaturation at 95 °C for 10 min and 40 cycles of15 sec melting at 95 °C and 1min annealing/extension at 60°C. Relative mRNA abundance was quantified using $2^{-\Delta\Delta CT}$ method. Each sample was analyzed three times and data averaged.

Glutathione depletion and cell survival assay
YS and control cells were plated into a 96 well plate at 2000-3000 cells per well. Cells were kept overnight at 37^0C and 5% CO_2 to allow attachment. Cells were treated with 0-100 μM BSO and incubated for 48 hours at 37^0C and 5% CO_2. BSO solution was renewed after 24 hours. Cells were washed after 48 hours with PBS and incubated with 120μl of solution containing 25μM PMS (phenazine methanosulfate) and 333μg/ml 3-(4,5-dimethylthiazol-2-yl)-5-(3-carboxy-methoxy-phenyl)-2-(4-sulfophenyl)-2H-tetrazolium (MTS), in DMEM without FBS. Cells were incubated for 20min, lysed with 50μl of 10% SDS and absorbance recorded at 490nm. Samples were measured in triplicates.

Statistical Analyses
Statistical analyses (comparisons between the experimental groups) were performed using Student's *t*-test (two-tailed, unpaired). *P* value <0.05 was considered to be statistically significant.

RESULTS

Copper is elevated in the intracellular compartments of *ATP7A*$^{-/-}$ cells. To understand consequences of ATP7A inactivation we used previously generated skin fibroblasts from MD patients, YS (immortalized), MF1 and MF2 cells (18,19) and control cells derived from one of the patients' mother or an unrelated male. The main set of experiments was done using the YS cells and control XS cells derived from a patient mother. The MF1 and MF2 cells and an additional control cell line (from an unrelated male) were utilized to verify our main observations. Consistent with previous reports (28,29), loss of ATP7A activity was associated with an increase in cellular copper content under basal growth conditions (Fig.1A). Higher copper accumulation in the patient cells compared to control was also evident following treatment of cells with low (5 μM) or high (100 μM) copper for 4 hour or 48 hours (Fig.1B, left and right panels, respectively).

Sub-cellular fractionation and ICP-MS analysis revealed that copper was elevated in all the major intracellular compartments (Fig.1C). In the nuclei, copper was higher on average, but the increase was not statistically significant; mitochondria had a 2.4 fold increase of copper content and the post-mitochondrial fraction, comprised of cytosol and microsomes, had a 2.6 fold higher copper. Accumulation was specific for copper with no changes detected for Mn, Ca, Fe and Zn (Fig.2). Thus, excess cytosolic copper enters the membrane-encapsulated nuclei and mitochondria, where it remains sequestered during cell fractionation.

The change in spatial distribution of copper was confirmed by X-ray fluorescence microscopy (Fig.3). In control cells, copper was highest in the vicinity of nuclei, but not in the nucleus, in agreement with previously published results (30). In patient cells, the pattern of copper distribution was altered. The perinuclear ring disappeared and copper was distributed throughout the cell and enriched within nuclei (Fig.3A). Higher copper content and changes in the intracellular distribution of copper in patient cells were associated with an increased expression of metallothioneins (MT1 and MT2) (Fig.3B). Under basal culture conditions the increase reflected moderate copper accumulation. Treatment with 5 μM or 100 μM copper for 48 hours further increased expression of MT1 and MT2, especially in YS cells, reflecting a higher copper load (Fig. 3C)

Probes for quantitative imaging of glutathione oxidation in sub-cellular compartments of live cells. Slight copper elevation and upregulation of

MT1,2 (which bind copper very tightly) raises the question whether the modest copper misbalance has any negative consequences for cell metabolism. Copper is a redox active metal and it may alter the redox environment of intracellular compartments. Two main systems maintain thiol redox balance, a glutathione (GSH)/glutathione disulfide (GSSG) couple and a reduced/oxidized thioredoxin couple (31,32). Conventional methods of measuring GSH:GSSG ratio involve cell lysis and oxidation artifacts (33). Consequently, to characterize the redox status of cell compartments in patient cells we used redox sensors and quantitative real-time imaging in live cells (Fig.4). For studies of GSH:GSSG ratio in the cytosol, we used a recently developed GRX1-roGFP2 sensor (21,34). To characterize the GSH:GSSG status in the nucleus, we added an SV-40 Nuclear Localization Signal (NLS) to the N-terminus of GRX1-roGFP2 (Fig.4A). To target the sensor to mitochondria, we fused a triple Mitochondria Target Sequence (MTS) from the subunit VIII of human cytochrome c oxidase to the GRX1-roGFP2 N-terminus (Fig.4A). This tag directed the sensor to the mitochondria matrix. Correct localization of the cytosolic and nuclear sensors was apparent from the characteristic patterns of fluorescence (Fig.4B). Targeting of MTS-GRX1-roGFP2 to mitochondria was confirmed by colocalization with MitoTracker Red (Fig.4B).

The ability of sensors to identify changes in glutathione oxidation was verified by treatment of cells with DTT or H_2O_2. Oxidation/reduction of glutathione causes reciprocal changes in the excitation spectrum of GRX1-roGFP2 at two characteristic wavelengths (405 nm and 488 nm). The ratio of fluorescence intensities emitted following excitation at 405 nm and 488 nm ($IR_{405/488nm}$) increases when glutathione is oxidized and decreases upon treatment with a reductant (Fig.4C). Each of the compartment-specific sensor showed higher $IR_{405/488}$ value in response to treatment of cells with 100 μM H_2O_2; the $IR_{405/488}$ value was decreased upon subsequent treatment with 500μM DTT (Fig.4C).

Patient cells show an increased glutathione oxidation, especially in mitochondria. We then used the sensors to characterize the status of glutathione pair in different compartments of control and patient cells. In control cells, the $IR_{405/488}$ values for cytosol and nucleus were similar indicating similar oxidation state of the glutathione pair in these two compartments (Fig.5 A and B). For mitochondria, $IR_{405/488}$ was lower compared to nucleus and cytosol, suggesting that glutathione was more reduced. This was unexpected, because mitochondria are known to contain large amounts of peroxide. To verify our conclusion we quantified fluorescence from approximately 50 cells in each of the five independent experiments, and obtained consistently low $IR_{405/488}$ values (Fig.5C). We have also measured the $IR_{405/488}$ value in different regions of mitochondria and found that in control cells, variation in sensor oxidation was small (Fig.5C).

For patient cells, the oxidation state of glutathione in cytosol and nuclei was similar and the $IR_{405/488}$ values did not differ significantly from the $IR_{405/488}$ values of the corresponding compartments in control cells (Fig.5B). Thus, copper accumulating in cytosol and nucleus is efficiently buffered and/or changes in glutathione oxidation are quickly corrected. In contrast, glutathione in YS mitochondria was significantly oxidized as evident from a higher $IR_{405/488}$ value (Fig.5AB) compared to control. Evaluation of various cells and different regions in mitochondria revealed that the maximum oxidation and variation in glutathione oxidation within the mitochondria were both significantly higher in the YS cells compared to control (Fig.5C). To verify that the observed differences in mitochondria glutathione balance were not restricted to YS cells or were caused by genomic differences between the YS and control cells, we examined redox status of mitochondria using different control cells and two MD patient cell lines (MF1, MF2). In both cases, MD mitochondria showed higher oxidation of GRX1-roGFP2 sensor (Fig.5D). Total levels of glutathione in cells and in isolated mitochondria fractions were similar for control and patient cells (Fig.5E and 5F). We attempted to test whether the change in the GSH:GSSG ratio in patient cells was caused by copper binding to GSH, which would make GSH unavailable for redox reactions. Treatment of mitochondria homogenates with a copper chelator, BCS, on average increased

available GSH however the increase was not statistically significant (Fig.5F).

Glutathione oxidation in mitochondria is reversed by expression of ATP7B. Mitochondria matrix is thought to have a "copper storage pool" in the form of a complex with a small ligand, CuL, which apparently renders copper inert (35). We hypothesized that in the absence of active ATP7A, copper that is normally transported into the secretory pathway, enters mitochondria matrix exceeding a buffering capacity of CuL and altering GSH:GSSG balance. Restoration of copper flow through the secretory pathway should prevent entry of unligated copper into mitochondria and restore the GSH:GSSG balance. To test this prediction, we co-transfected YS cells with MTS-GRX1-roGFP2 and mCherry-ATP7B (Fig.6 left panel). We used ATP7B, instead of ATP7A, for technical reasons. (The ability of ATP7B to substitute ATP7A in YS cells was previously demonstrated (17,36-38)). In cells expressing ATP7B, the $IR_{405/488}$ value was lower compared to cells lacking ATP7B (Fig 6, right panel), indicating that the restoration of the copper flux to the secretory pathway alone restored the mitochondrial glutathione balance, presumably by removing excess copper.

Effect of ATP7A inactivation on mitochondria redox balance is species-independent. To test how general is the effect of ATP7A on the GSH:GSSG pair in mitochondria we selected different cells (3T3-L1 preadipocytes, which express ATP7A but not ATP7B) from different species (mouse) and inactivated ATP7A using CRISPR/Cas9 system. The deletions in both alleles of *ATP7A* gene were confirmed by sequencing (Fig. 7A). The mutation resulted in a frame shift and a loss of ATP7A expression (Fig. 7B). Similarly to human cell, the ability of ATP7A-deficient cells to proliferate in the basal media was not negatively impacted. As expected, Cu levels in $ATP7A^{-/-}$ cells were elevated compared to control 3T3-L1 cells (Fig. 7C). Expression of MTS-GRX1-roGFP2 sensor revealed higher sensor oxidation (higher $IR_{405/488}$ value) in mitochondria of cells lacking ATP7A compared to control 3T3-L1 cells (Fig. 7D,E), similarly to human $ATP7A^{-/-}$ (YS) cells.

H_2O_2 levels are higher in patient mitochondria. The above data indicated that accumulating copper altered glutathione balance in mitochondria matrix but the mechanism remained unclear. Elevated copper may directly affect (bind to or oxidize) glutathione, or it may increase production of reactive oxygen species, resulting in accumulation of peroxide. To measure levels of peroxide, we took advantage of the genetically encoded ratiometric peroxide sensors (HyPer) targeted to cytosol, nucleus and mitochondria (22), (39). The $IR_{488/405}$ ratio of fluorescence produced by the sensors is directly proportional to H_2O_2 levels. In control cells, peroxide was highest in mitochondria, as expected; the cytosol contained intermediate levels of peroxide, and the levels of H_2O_2 in nuclei were low (Fig. 8A). ATP7A inactivation and copper accumulation did not significantly change peroxide content in the nucleus but increased cytosolic peroxide by 44.16%. Most significant increase (59%) was detected in mitochondria (Fig. 8B). We also found that a larger fraction of thioredoxin (TRX1) was oxidized in YS cells in basal conditions compared to control, and that TRX1 became fully oxidized when cells were treated with excess copper (Fig.8C). Thus, both redox systems in the MD patients' mitochondria are compromised and the levels of peroxide are higher than in control.

Glutathione oxidation in mitochondria is independent of H_2O_2 levels

Copper can facilitate production of superoxide with consequent generation of peroxide or it can oxidize GSH decreasing the ability of GSH-dependent enzymes to eliminate H_2O_2. To discriminate between these possibilities, we used MitoQ, an antioxidant specifically targeted to mitochondria (40-42). Treatment of YS cells expressing HyPer-Mito with MitoQ, decreased the $IR_{488/405}$ value in YS mitochondria indicative of lower H_2O_2 content compared to cells treated with an equivalent volume of ethanol (vehicle) (Fig.9A). The decrease in oxidative burden by MitoQ was further demonstrated by measuring mRNA levels for IFI27, a mitochondria resident protein, expression of which is influenced by oxidative stress (43). Treatment with MitoQ upregulated IFI27 mRNA levels in both control cells and the YS cells (Fig.9C), consistent with the sequestration of peroxide. The treatment, however,

did not change status of glutathione pair as evidenced by an unchanged oxidation of MTS-GRX1-roGFP2 (Fig.9B). Thus, although MitoQ diminishes mitochondria H_2O_2, glutathione remains oxidized. This result suggests that elevation of H_2O_2 occurs downstream of glutathione and that glutathione is the primary (and/or independent of peroxide) target of elevated copper.

Redox misbalance markedly sensitized cells to a decrease in total glutathione. Oxidative stress may trigger mitochondria fission and decrease activity of respiratory chain. Consequently, to determine functional consequences of redox misbalance in MD patients' mitochondria, we characterized mitochondria morphology and function. Electron microscopy of control and patient cells showed no significant differences in the mitochondria length, shape, or cristae' appearance (Fig.10A). The activity of cytochrome C oxidase in freshly prepared mitochondria also did not differ significantly from the control (Fig 10B). We hypothesized that under basal conditions mitochondria of ATP7A-deficient cells retain sufficient redox buffering capacity, which (given a negative effect of copper on GSH) would greatly depend on total available glutathione. To test this hypothesis, we treated the YS and control cells with different concentrations of the glutathione synthase inhibitor, BSO (2.5-100 μM) to decrease levels of cellular glutathione. Cell viability was quantified by the MTS assay, which calculates mitochondria functional integrity. Viability of control cells was unchanged in the presence of 2.5 μM BSO, whereas the number of live YS cells decreased to 37%. At higher inhibitor concentrations, the YS cells were not viable illustrating loss of their mitochondria function upon decreasing glutathione levels.

Discussion

ATP7A is the major copper transporter with an established role in a dietary copper uptake and the delivery of copper to such important enzymes as dopamine-β-hydroxylase, peptidyl-α-mono-oxygenase, lysyl oxidase, SOD3 and others. Here we demonstrate that normal ATP7A transport activity is essential for maintaining the redox balance in mitochondria. This function is mediated through the sequestration of exchangeable "active" copper within the secretory pathway. The exchangeable copper, which enters the mitochondria when ATP7A is inactivated, decreases the ratio of reduced-to-oxidized glutathione and increases levels of peroxide and protein oxidation. Copper may act by binding to GSH and thus lowering amount of reduced glutathione, which in turn may decrease the activity of glutathione peroxidase and increase levels of peroxide. High sensitivity of MD cells to glutathione depletion and enhanced oxidation of thioredoxin are consistent with this scenario. More complex mechanisms could also be at play. In the liver, copper accumulation changes activity of nuclear receptors, triggers changes in RNA splicing machinery, alters DNA methylation, and disregulates lipid metabolism(44-50). Systematic analysis of how redox misbalance contributes to the transcriptional, proteomic, and metabolic changes in cells and individual compartments would help to generate a comprehensive picture of cellular response to copper overload.

The effects of copper in MD cells are observed under basal growth conditions when copper elevation is modest. This suggests that the copper-buffering capacity of mitochondria matrix is limited and it is unlikely to function as a copper storage pool for the entire cell. The low molecular weight copper ligand CuL that binds copper in the mitochondria matrix could be a specialized copper reservoir necessary for an uninterrupted biosynthesis of functional cytochrome c oxidase (35).

The observed marked effect of ATP7A inactivation on mitochondria copper content and redox environment was somewhat unexpected, since copper accumulation in MD fibroblasts has traditionally been considered mainly cytosolic. Sensitivity of mitochondria to high copper has been previously reported for Wilson disease and animal models of copper overload (51-53) and is thought to be an important component of disease pathology in copper overload states. Different sensitivity of redox environment of cellular compartments to copper elevation raises many new questions. Does copper act differently in different cellular compartments, i.e. through binding to proteins/DNA in the nuclei and changes of redox buffers in mitochondria? Does redox

misbalance in mitochondria yield metabolic changes that in turn trigger epigenetic changes in the nuclei? Response of which cellular compartment is more significant to cell adaptation to oxidative stress and cell survival? How compartemtal responses are integrated? We speculate that mitochondria might be particularly susceptible to elevated copper, because they lack dedicated protein chelators such as metallothioneins and the transport/folding of proteins localized to the intermembrane space is mediated by the unique redox-dependent MIA pathway.

To date, most efforts in developing therapeutics for Menkes disease have been directed towards increasing copper delivery to and utilization in the CNS. Brain copper deficiency accounts for many of the neurological manifestations of classic Menkes disease. Our work adds a new dimension to a complex set of consequences associated with ATP7A inactivation. In addition to a well-established loss of activity of copper-dependent enzymes in the secretory pathway, we demonstrate dysregulation of the redox balancing system in mitochondria of ATP7A-deficient fibroblasts that hyper-accumulate Cu due to impaired egress. The effect on mitochondria redox environment, and presumably function of various redox dependent enzymes, may be relevant in peripheral tissues of Menkes patients where copper accumulates (e.g., kidney and intestine among them). Tissues and cells with a relatively low glutathione content or high demand for robust mitochondria function (such as heart and skeletal muscle) could also be adversely affected. Further clinical and laboratory investigations in animal models are warranted to better understand this phenomenon and its full implications.

Acknowledgements
We thank Dr Ann Hubbard (Johns Hopkins University School of Medicine) for XS and YS cells; Dr Tobias P. Dick (German Cancer Research Center (DKFZ), Heidelberg) for GRX1-roGFP2 construct; Dr Vadim Gladyshev (Brigham and Women's Hospital, Harvard Medical School) for HyPer constructs. The Elemental Analysis Core at OHSU has performed ICP-MS measurements. We acknowledge use of the Advanced Photon Source at Argonne National Laboratory, supported by the U.S. Department of Energy, Office of Science, Office of Basic Energy Sciences, under contract number, DE-AC02-06CH11357. The work was financially supported by National Institute of Health 5R01GM101502 to SL, GM090016 and instrumentation grant RR025512 to MR and R01NS072241 to M.J.W. Ramanujan Fellowship SB/S2/RJN-106/2015, SERB, Department of Science & Technology, to AB is gratefully acknowledged. We thank staff of Johns Hopkins SOM MicFac facility for help with EM samples sectioning and staining.

Conflict of Interest
The authors declare no conflicts of interest related to the contents of this article.

Authors Contributions
MR and AB - involved in designing of experiments, acquisition of data, data analysis and interpretation and writing the manuscript, SL – involved in designing of experiments, data analysis and interpretation, and writing the manuscript, MD, ER, AC, YL, TC – involved in acquisition of data, LB – involved in analysis and interpretation of data, MPM, LY, SGK – provided critical reagents for the study, read and commented on the manuscript

REFERENCES
1. Menkes, J. H., Alter, M., Steigleder, G. K., Weakley, D. R., and Sung, J. H. (1962) A sex-linked recessive disorder with retardation of growth, peculiar hair, and focal cerebral and cerebellar degeneration. *Pediatrics* **29**, 764-779
2. Vulpe, C., Levinson, B., Whitney, S., Packman, S., and Gitschier, J. (1993) Isolation of a candidate gene for Menkes disease and evidence that it encodes a copper-transporting ATPase. *Nature genetics* **3**, 7-13

3. Maryon, E. B., Molloy, S. A., and Kaplan, J. H. (2013) Cellular glutathione plays a key role in copper uptake mediated by human copper transporter 1. *American journal of physiology. Cell physiology* **304**, C768-779
4. Kaler, S. G. (2011) ATP7A-related copper transport diseases-emerging concepts and future trends. *Nature reviews. Neurology* **7**, 15-29
5. Grimes, A., Hearn, C. J., Lockhart, P., Newgreen, D. F., and Mercer, J. F. (1997) Molecular basis of the brindled mouse mutant (Mo(br)): a murine model of Menkes disease. *Human molecular genetics* **6**, 1037-1042
6. La Fontaine, S., Theophilos, M. B., Firth, S. D., Gould, R., Parton, R. G., and Mercer, J. F. (2001) Effect of the toxic milk mutation (tx) on the function and intracellular localization of Wnd, the murine homologue of the Wilson copper ATPase. *Human molecular genetics* **10**, 361-370
7. Mercer, J. F., Grimes, A., Ambrosini, L., Lockhart, P., Paynter, J. A., Dierick, H., and Glover, T. W. (1994) Mutations in the murine homologue of the Menkes gene in dappled and blotchy mice. *Nature genetics* **6**, 374-378
8. Hodgkinson, V. L., Dale, J. M., Garcia, M. L., Weisman, G. A., Lee, J., Gitlin, J. D., and Petris, M. J. (2015) X-linked spinal muscular atrophy in mice caused by autonomous loss of ATP7A in the motor neuron. *J Pathol* **236**, 241-250
9. La Fontaine, S., Ackland, M. L., and Mercer, J. F. (2010) Mammalian copper-transporting P-type ATPases, ATP7A and ATP7B: emerging roles. *Int J Biochem Cell Biol* **42**, 206-209
10. Liu, P. C., Chen, Y. W., Centeno, J. A., Quezado, M., Lem, K., and Kaler, S. G. (2005) Downregulation of myelination, energy, and translational genes in Menkes disease brain. *Molecular genetics and metabolism* **85**, 291-300
11. Lenartowicz, M., Sasula, K., and Zawadowska, B. (2001) Alterations in kidney morphology in mice with mosaic mutation. *Folia Histochem Cytobiol* **39**, 275-281
12. Kodama, H., Sato, E., Gu, Y. H., Shiga, K., Fujisawa, C., and Kozuma, T. (2005) Effect of copper and diethyldithiocarbamate combination therapy on the macular mouse, an animal model of Menkes disease. *J Inherit Metab Dis* **28**, 971-978
13. Lenartowicz, M., Windak, R., Tylko, G., Kowal, M., and Styrna, J. (2010) Effects of copper supplementation on the structure and content of elements in kidneys of mosaic mutant mice. *Biol Trace Elem Res* **136**, 204-220
14. Nomura, S., Nozaki, S., Hamazaki, T., Takeda, T., Ninomiya, E., Kudo, S., Hayashinaka, E., Wada, Y., Hiroki, T., Fujisawa, C., Kodama, H., Shintaku, H., and Watanabe, Y. (2014) PET imaging analysis with 64Cu in disulfiram treatment for aberrant copper biodistribution in Menkes disease mouse model. *J Nucl Med* **55**, 845-851
15. Du, T., La Fontaine, S. L., Abdo, M., Bellingham, S. A., Greenough, M., Volitakis, I., Cherny, R. A., Bush, A. I., Hudson, P. J., Camakaris, J., Mercer, J. F., Crouch, P. J., Masters, C. L., Perreau, V. M., and White, A. R. (2008) Investigating copper-regulated protein expression in Menkes fibroblasts using antibody microarrays. *Proteomics* **8**, 1819-1831
16. Leary, S. C., Cobine, P. A., Nishimura, T., Verdijk, R. M., de Krijger, R., de Coo, R., Tarnopolsky, M. A., Winge, D. R., and Shoubridge, E. A. (2013) COX19 mediates the transduction of a mitochondrial redox signal from SCO1 that regulates ATP7A-mediated cellular copper efflux. *Molecular biology of the cell* **24**, 683-691
17. Guo, Y., Nyasae, L., Braiterman, L. T., and Hubbard, A. L. (2005) NH2-terminal signals in ATP7B Cu-ATPase mediate its Cu-dependent anterograde traffic in polarized hepatic cells. *American journal of physiology. Gastrointestinal and liver physiology* **289**, G904-916
18. Kaler, S. G., Buist, N. R., Holmes, C. S., Goldstein, D. S., Miller, R. C., and Gahl, W. A. (1995) Early copper therapy in classic Menkes disease patients with a novel splicing mutation. *Ann Neurol* **38**, 921-928
19. Kaler, S. G., Das, S., Levinson, B., Goldstein, D. S., Holmes, C. S., Patronas, N. J., Packman, S., and Gahl, W. A. (1996) Successful early copper therapy in Menkes disease associated with a mutant transcript containing a small In-frame deletion. *Biochem Mol Med* **57**, 37-46

20. Vogt, S. (2003) Maps: A set of software tools for analysis and visualization of 3D X-ray fluorescent datasets. *Journal De Physique IV* **104**, 635-638
21. Gutscher, M., Pauleau, A. L., Marty, L., Brach, T., Wabnitz, G. H., Samstag, Y., Meyer, A. J., and Dick, T. P. (2008) Real-time imaging of the intracellular glutathione redox potential. *Nature methods* **5**, 553-559
22. Malinouski, M., Zhou, Y., Belousov, V. V., Hatfield, D. L., and Gladyshev, V. N. (2011) Hydrogen peroxide probes directed to different cellular compartments. *PloS one* **6**, e14564
23. Anderson, M. E. (1985) Determination of glutathione and glutathione disulfide in biological samples. *Methods in enzymology* **113**, 548-555
24. Watson, W. H., Pohl, J., Montfort, W. R., Stuchlik, O., Reed, M. S., Powis, G., and Jones, D. P. (2003) Redox potential of human thioredoxin 1 and identification of a second dithiol/disulfide motif. *The Journal of biological chemistry* **278**, 33408-33415
25. Bersani, N. A., Merwin, J. R., Lopez, N. I., Pearson, G. D., and Merrill, G. F. (2002) Protein electrophoretic mobility shift assay to monitor redox state of thioredoxin in cells. *Methods in enzymology* **347**, 317-326
26. Mali, P., Yang, L., Esvelt, K. M., Aach, J., Guell, M., DiCarlo, J. E., Norville, J. E., and Church, G. M. (2013) RNA-guided human genome engineering via Cas9. *Science (New York, N.Y.)* **339**, 823-826
27. Rodriguez, S., and Wolfgang, M. J. (2012) Targeted chemical-genetic regulation of protein stability in vivo. *Chemistry & biology* **19**, 391-398
28. Goka, T. J., Stevenson, R. E., Hefferan, P. M., and Howell, R. R. (1976) Menkes disease: a biochemical abnormality in cultured human fibroblasts. *Proceedings of the National Academy of Sciences of the United States of America* **73**, 604-606
29. Royce, P. M., Camakaris, J., and Danks, D. M. (1980) Reduced lysyl oxidase activity in skin fibroblasts from patients with Menkes' syndrome. *The Biochemical journal* **192**, 579-586
30. Ralle, M., Huster, D., Vogt, S., Schirrmeister, W., Burkhead, J. L., Capps, T. R., Gray, L., Lai, B., Maryon, E., and Lutsenko, S. (2010) Wilson disease at a single cell level: intracellular copper trafficking activates compartment-specific responses in hepatocytes. *The Journal of biological chemistry* **285**, 30875-30883
31. Holmgren, A., Johansson, C., Berndt, C., Lonn, M. E., Hudemann, C., and Lillig, C. H. (2005) Thiol redox control via thioredoxin and glutaredoxin systems. *Biochemical Society transactions* **33**, 1375-1377
32. Jones, D. P. (2006) Disruption of mitochondrial redox circuitry in oxidative stress. *Chemico-biological interactions* **163**, 38-53
33. Rota, C., Chignell, C. F., and Mason, R. P. (1999) Evidence for free radical formation during the oxidation of 2'-7'-dichlorofluorescin to the fluorescent dye 2'-7'-dichlorofluorescein by horseradish peroxidase: possible implications for oxidative stress measurements. *Free radical biology & medicine* **27**, 873-881
34. Morgan, B., Sobotta, M. C., and Dick, T. P. (2011) Measuring E(GSH) and H2O2 with roGFP2-based redox probes. *Free radical biology & medicine* **51**, 1943-1951
35. Cobine, P. A., Pierrel, F., Bestwick, M. L., and Winge, D. R. (2006) Mitochondrial matrix copper complex used in metallation of cytochrome oxidase and superoxide dismutase. *The Journal of biological chemistry* **281**, 36552-36559
36. Petris, M. J., Strausak, D., and Mercer, J. F. (2000) The Menkes copper transporter is required for the activation of tyrosinase. *Human molecular genetics* **9**, 2845-2851
37. Gupta, A., Bhattacharjee, A., Dmitriev, O. Y., Nokhrin, S., Braiterman, L., Hubbard, A. L., and Lutsenko, S. (2011) Cellular copper levels determine the phenotype of the Arg875 variant of ATP7B/Wilson disease protein. *Proceedings of the National Academy of Sciences of the United States of America* **108**, 5390-5395
38. Schushan, M., Bhattacharjee, A., Ben-Tal, N., and Lutsenko, S. (2012) A structural model of the copper ATPase ATP7B to facilitate analysis of Wilson disease-causing mutations and studies of the transport mechanism. *Metallomics : integrated biometal science* **4**, 669-678

39. Belousov, V. V., Fradkov, A. F., Lukyanov, K. A., Staroverov, D. B., Shakhbazov, K. S., Terskikh, A. V., and Lukyanov, S. (2006) Genetically encoded fluorescent indicator for intracellular hydrogen peroxide. *Nature methods* **3**, 281-286
40. Marthandan, S., Murphy, M. P., Billett, E., and Barnett, Y. (2011) An investigation of the effects of MitoQ on human peripheral mononuclear cells. *Free radical research* **45**, 351-358
41. Pletjushkina, O. Y., Fetisova, E. K., Lyamzaev, K. G., Ivanova, O. Y., Domnina, L. V., Vyssokikh, M. Y., Pustovidko, A. V., Alexeevski, A. V., Alexeevski, D. A., Vasiliev, J. M., Murphy, M. P., Chernyak, B. V., and Skulachev, V. P. (2006) Hydrogen peroxide produced inside mitochondria takes part in cell-to-cell transmission of apoptotic signal. *Biochemistry. Biokhimiia* **71**, 60-67
42. Kelso, G. F., Porteous, C. M., Coulter, C. V., Hughes, G., Porteous, W. K., Ledgerwood, E. C., Smith, R. A., and Murphy, M. P. (2001) Selective targeting of a redox-active ubiquinone to mitochondria within cells: antioxidant and antiapoptotic properties. *The Journal of biological chemistry* **276**, 4588-4596
43. Williams, T. D., Diab, A., Ortega, F., Sabine, V. S., Godfrey, R. E., Falciani, F., Chipman, J. K., and George, S. G. (2008) Transcriptomic responses of European flounder (Platichthys flesus) to model toxicants. *Aquat Toxicol* **90**, 83-91
44. Hamilton, J. P., Koganti, L., Muchenditsi, A., Pendyala, V. S., Huso, D., Hankin, J., Murphy, R. C., Huster, D., Merle, U., Mangels, C., Yang, N., Potter, J. J., Mezey, E., and Lutsenko, S. (2015) Activation of LXR/RXR pathway ameliorates liver disease in atp7b (wilson disease) mice. *Hepatology (Baltimore, Md.)*
45. Wooton-Kee, C. R., Jain, A. K., Wagner, M., Grusak, M. A., Finegold, M. J., Lutsenko, S., and Moore, D. D. (2015) Elevated copper impairs hepatic nuclear receptor function in Wilson's disease. *The Journal of clinical investigation* **125**, 3449-3460
46. Burkhead, J. L., Ralle, M., Wilmarth, P., David, L., and Lutsenko, S. (2011) Elevated copper remodels hepatic RNA processing machinery in the mouse model of Wilson's disease. *Journal of molecular biology* **406**, 44-58
47. Wilmarth, P. A., Short, K. K., Fiehn, O., Lutsenko, S., David, L. L., and Burkhead, J. L. (2012) A systems approach implicates nuclear receptor targeting in the Atp7b(-/-) mouse model of Wilson's disease. *Metallomics : integrated biometal science* **4**, 660-668
48. Roberts, E. A., Robinson, B. H., and Yang, S. (2008) Mitochondrial structure and function in the untreated Jackson toxic milk (tx-j) mouse, a model for Wilson disease. *Molecular genetics and metabolism* **93**, 54-65
49. Medici, V., Shibata, N. M., Kharbanda, K. K., Islam, M. S., Keen, C. L., Kim, K., Tillman, B., French, S. W., Halsted, C. H., and LaSalle, J. M. (2014) Maternal choline modifies fetal liver copper, gene expression, DNA methylation, and neonatal growth in the tx-j mouse model of Wilson disease. *Epigenetics* **9**, 286-296
50. Huster, D., Purnat, T. D., Burkhead, J. L., Ralle, M., Fiehn, O., Stuckert, F., Olson, N. E., Teupser, D., and Lutsenko, S. (2007) High copper selectively alters lipid metabolism and cell cycle machinery in the mouse model of Wilson disease. *The Journal of biological chemistry* **282**, 8343-8355
51. Roberts, E. A., Robinson, B. H., and Yang, S. (2008) Mitochondrial structure and function in the untreated Jackson toxic milk (tx-j) mouse, a model for Wilson disease. *Mol Genet Metab* **93**, 54-65
52. Zischka, H., Lichtmannegger, J., Schmitt, S., Jagemann, N., Schulz, S., Wartini, D., Jennen, L., Rust, C., Larochette, N., Galluzzi, L., Chajes, V., Bandow, N., Gilles, V. S., DiSpirito, A. A., Esposito, I., Goettlicher, M., Summer, K. H., and Kroemer, G. (2011) Liver mitochondrial membrane crosslinking and destruction in a rat model of Wilson disease. *J Clin Invest* **121**, 1508-1518
53. Sheline, C. T., and Choi, D. W. (2004) Cu2+ toxicity inhibition of mitochondrial dehydrogenases in vitro and in vivo. *Ann Neurol* **55**, 645-653

Abbreviations

BCS - Bathocuproine disulfonate, BSO - Buthionine sulfoximine; MitoQ - Phosphonium, [10-(4,5-dimethoxy-2-methyl-3,6-dioxo-1,4-cyclohexadien- 1-yl)decyl]triphenyl-, methanesulfonate

Figure Legends

Figure 1. Copper redistribution in control and MND patient cells. *Panel A left:* Copper levels in cells from the patient mother (control) and MND patient (YS) under basal condition (108.7 ± 59.6 μM and 182.4 ± 57.4 μM, respectively, ***p-value* 0.0067) and in response to treatment with 100 μM $CuCl_2$ for 4 hours (222.8 ± 91.3 μM and 376.7 ± 138.5 μM, respectively, **p-value* 0.0290). *Panel A right:* Copper levels under basal conditions in cells from an independent control/unrelated male (7.24±0.78 ng/10^6 cells) and MND patient (MF1-34.33±5.52 ng/10^6 cells, MF2-15.7±2.17 ng/10^6 cells; ****p-value* 0.0005, ***p-value* 0.0031). *Panel B:* MND cells accumulate more copper in response to treatment with low (5 μM) or high (100μM) $CuCl_2$ when compared to control cells. *Left panel:* Copper levels in YS cells and control cells in basal medium (191.60±15.86μM and 107.56±26.68 μM, respectively, (***p-value* 0.009), low copper (245.70±29.87μM and 142.70±17.98 μM, respectively, ***p-value* 0.008) and high copper (376.76±48.95 μM and 185.37±24.09 μM, respectively, **p-value* 0.03) after 4 hours of treatment. *Right panel*: Copper levels in YS and control cells in basal medium (156.43±20.59 μM and 90.17±18.07 μM, respectively *p-value 0.03) low copper (1158.20±205.90 μM and 557.20±167.75 μM, respectively, ns *p-value* 0.15) and high copper (2403.65±211.07 μM and 1171.35±130.15 μM, respectively, ****p-value* 0.0003) after 48 hours of treatment. *Panel C*: Copper levels in subcellular fractions of control and YS cells. Mitochondria (17±5.57 ng/mg protein and 41±4.36 ng/mg protein in control and YS, respectively), nuclei (12±3.46 ng/mg protein and 23.33±11.93 ng/mg protein); post mitochondria - 33±13.11 ng/mg and 84.67±19.22 ng/mg protein) ***p-value* 0.0091, ***p-value* 0.0071. In all panels, data are means ± SD, three independent experiments.

Figure 2. Levels of metals other than copper are unchanged in subcellular fractions of control and YS cells. The values for Mn in nuclear extracts were variable (1.7-5.9 ng/mg protein for control cells and 3.8-11.7 ng/mg protein for YS cells) in contrast to other metals, which were measured in parallel using ICP-MS and yielded consistent values. Although there is an apparent trend to higher mean values in YS cells, the difference was not statistically significant. Mean and SD data from 3 independent experiments are shown.

Figure 3. Change in intracellular distribution of copper in YS cells is associated with up-regulation of metallothioneins. *Panel A*: XFM images for control and YS cells grown under basal conditions. Visible light microscope images and elemental maps for P, S, Fe, Cu and Zn. The relative elemental concentration is presented by false coloring (temperature bar), the scale bar is 20 μm. N denotes the position of the nucleus. *Panel B*: Relative expression of metallothionein 1 (MT1) in YS is 1.35 fold higher that in control cells under basal condition (*** p-value 0.0011). *Panel C*: Increase in the levels of metallothioneins (MT1 and MT2) transcripts in control and YS cells in response to treatment with 100 μM $CuCl_2$ for 48 hours; values are given in comparison to basal conditions (Data are means ±SD, n=3)

Figure 4. Probes for measuring the GSH:GSSG ratio in cellular compartments. *Panel A:* Cartoon showing design of the GRX1-roGFP2-based sensors targeted to cytosol (GRX1-roGFP2), nucleus (NNLS-GRX1-roGFP2) and mitochondria (MTS-GRX1-roGFP2); NLS – Nuclear Localisation Signal, MTS – Mitochondria Target Signal. *Panel B:* expression and subcellular localization of sensors. Diffuse pattern indicates cytosolic localization of GRX1-roGFP2; NNLS-GRX1-roGFP2 is targeted to nuclei; targeting of MTS-GRX1-roGFP2 (green) to mitochondria is verified by colocalization with Mitotracker (red). *Panel C left:* The ratiometric false color image of HEK293T cells expressing different sensors under basal condition and their response to treatment with 100μM H_2O_2 and 500μM DTT. *Panel C right:* Representative changes in $IR_{405/488}$ values in a single cell. Arrows indicate time at which oxidant and reductant were added.

Figure 5. Copper accumulation in YS cells is associated with increased oxidation of glutathione in mitochondria. *Panel A:* Ratiometric false colored image showing $IR_{405/488}$ in YS and control cells for different compartments. YS cells have higher $IR_{405/488}$ value than in control cells (0.36±0.078 and 0.22±0.049) in mitochondria (MTS-GRX1-roGFP2) and no change in the cytosol (GRX1-roGFP2) or nuclei (NLS-GRX1-roGFP2). Cells were imaged at 40x magnification for GRX1-roGFP2 and NLS-GRX1-roGFP2 and at 63x magnification for MTS-GRX1-roGFP2. *Panel B:* Average $IR_{405/488}$ for different compartments in control and YS cells (****p-value*<0.001). *Panel C:* Range of $IR_{405/488}$ values determined by analysis of different regions of mitochondria within the same cell. *Panel D:* Average percent oxidation of MTS-GRX1-roGFP2 in control and Menkes fibroblasts (MF1 and MF2) cells (**p-*value* 0.006, **p-value* 0.0231). *Panel E:* GSH level in control and YS cells *Panel F:* GSH level in the mitochondria isolated from control and YS cells grown under basal conditions or treated with BCS. *ns *p-value* 0.3715, **ns *p-value* 0.6543. Average data from 5 replicate experiments (n=5) and 10 cells from each experiment have been represented.

Figure 6. Rescue of mitochondria glutathione redox misbalance in YS cells by expression of ATP7B. *Panel A:* YS cells were co-transfected with MTS-GRX1-roGFP2 (green) and mCherry-ATP7B (red). Merged image shows cells expressing only MTS-GRX1-roGFP2 (green) and coexpressing both MTS-GRX1-roGFP2 (green) and mCherry-ATP7B (red). Representative ratiometric image on the right shows that the $IR_{405/488}$ values in an YS cell (0.36±0.082) is higher than in the neighboring YS cells expressing mCherry-ATP7B (0.25±0.063). Cells expressing MTS-GRX1-roGFP2 have higher ratio than cells expressing both proteins. *Panel B*: Graph shows average $IR_{405/488}$ values in both cell types (****p-value<0.0001). Average data from 3 independent experiments with results from 10 cells per condition in each experiment are shown.

Figure 7. Deletion of ATP7A in 3T3-L1 pre-adipocytes is associated with elevation of cellular copper content and increased oxidation of glutathione in mitochondria. *Panel A:* CRISPR/CAS9-targeting of exon 2 generated deletion in both alleles of genomic *ATP7A* in 3T3-L1 cells. *Panel B:* Western blot analysis of cell lysates shows presence of ATP7A in the wild type (WT) 3T3-L1 cells and a loss of ATP7A expression in the CRISPR/CAS9 targeted 3T3-L1 cells; α-tubulin is used as a loading control. *Panel C:* Copper levels in wild type (3.4±0.49 ng/mg protein) and $ATP7A^{-/-}$ 3T3-L1 (10.32±0.41 ng/mg protein) cells under basal condition (****p-value < 0.0001; n=3). *Panel D:* Ratiometric ($IR_{405/488}$) false colored image of MTS-GRX1-roGFP2 fluorescence in WT and $ATP7A^{-/-}$ 3T3-L1. Cells were imaged at 40X magnification. *Panel E:* Oxidation of MTS-GRX1-roGFP2 in mitochondria of wild type (28.08±17.39, n=20 cells) and $ATP7A^{-/-}$ 3T3-L1 cells (44.90±20.73, n=28 cells) (***p value* 0.0049; data are means ±SEM of three independent experiments)

Figure 8. High H_2O_2 and thioredoxin oxidation in the cellular compartments of YS cells. *Panel A:* Representative ratiometric false colored images of HyPer sensors targeted to different cellular compartments in control and YS cells. *Panel B:* YS cells have higher $IR_{488/405}$ values for mitochondria-targeted sensor compared to control cells (2.89±0.67 and 1.82±0.33, respectively) and for the sensor targeted to cytosol (1.14±0.47 and 0.79±0.23, respectively). Data are means ±SD from five independent experiments with 10 cells in each condition in each experiment (****p-value<0.0001, *p-value 0.0202). *Pane C left*: Representative immunoblot of thioredoxin in control and YS cells grown under basal condition and either untreated or treated with 100 μM $CuCl_2$. Arrows indicates oxidized and reduced thioredoxin bands; treatment of the mitochondria lysates with DTT or H_2O_2 was done to generate a fully reduced and oxidized thioredoxin, respectively to be used as reference. *Panel C right:* Averaged ratio of reduced to oxidized thioredoxin in control (2.15±0.2) and YS cells (1.44±0.35) under basal condition and in response to treatment with 100 μM $CuCl_2$ (control – 0.83±0.62, YS – 0.06±0.13) Data are means ±SD, n=3, **p-value 0.0177, *p-value 0.039.

Figure 9. MitoQ decreases the peroxide content in YS cells but does not reverse glutathione oxidation. The patient **(**YS) cells expressing the HyPer-Mito sensor (Panel A) or the MTS-GRX1-roGFP2 sensor (Panel B) were treated either with MitoQ or equivalent volume of ethanol (vehicle). Ratiometric false color-coded images of sensors fluorescence are shown on the left (Panels A and B). The bar graph on the right of panel A illustrates the decrease of the $IR_{488/405}$ values of the Hyper sensor in response to MitoQ indicative of decreased levels of peroxide. The bar graph on the right of panel B illustrates the lack of changes in the $IR_{405/488}$ value for MTS-GRX1-roGFP2 sensor, i.e. MitoQ treatment does not affect glutathione oxidation. Experiment was repeated three times with 25 cells analyzed in each experiment. *Panel C:* Relative IFI27 expression in YS and control cells measured by real-time PCR before and after treatment with MitoQ (**** p-value<0.0001; data are means ±SD, n=3).

Figure 10. MND patient fibroblasts are highly sensitive to glutathione depletion in the absence of significant changes in mitochondria morphology and function. *Panel A*: Electron microscopy of control and MND patient cells (MF1 and MF2) grown under basal conditions illustrates similar mitochondrial morphology. *Panel B*: Cytochrome c oxidase activity is similar in mitochondria freshly isolated from the control and MND patient (YS) cells (ns *p-value*=0.2525; n=3). *Panel C*: Inhibition of glutathione synthesis has markedly different effects on viability of control and MND patient cells. The YS and control cells were plated at 2000 cells/well density and treated with increasing concentrations of BSO, an inhibitor of glutathione synthase, washed and stained with MTS (Data are means ± SD, n=3)

Figure 1

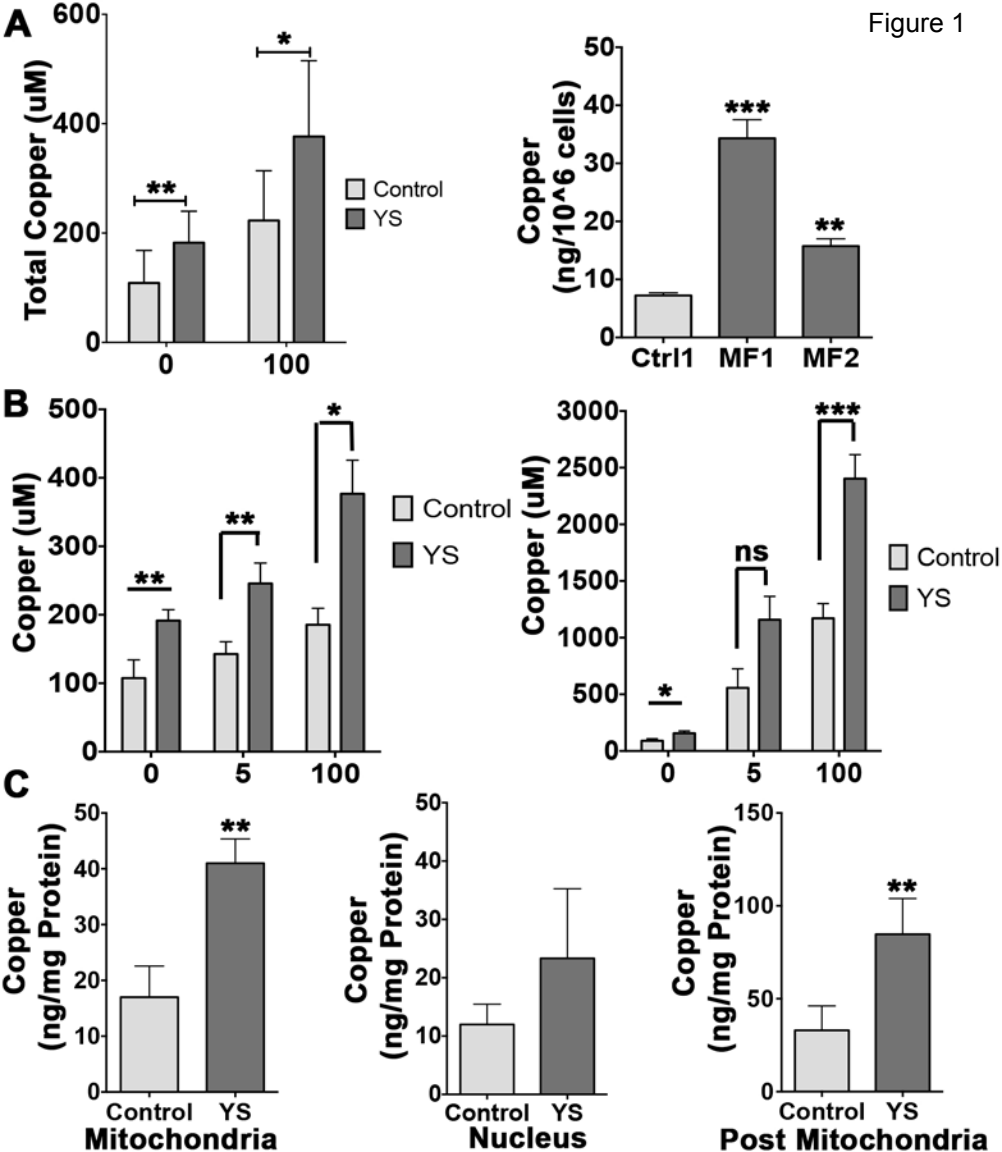
A
Total Copper (uM)
600
400
200
0
**
*
Control
YS
0
100
Copper (ng/10^6 cells)
50
40
30
20
10
0
***
**
Ctrl1
MF1
MF2
B
Copper (uM)
500
400
300
200
100
0
**
**
*
Control
YS
0
5
100
Copper (uM)
3000
2500
2000
1500
1000
500
0
*
ns
***
Control
YS
0
5
100
C
Copper (ng/mg Protein)
50
40
30
20
10
0
**
Control
YS
Mitochondria
Copper (ng/mg Protein)
50
40
30
20
10
0
Control
YS
Nucleus
Copper (ng/mg Protein)
150
100
50
0
**
Control
YS
Post Mitochondria

Figure 2

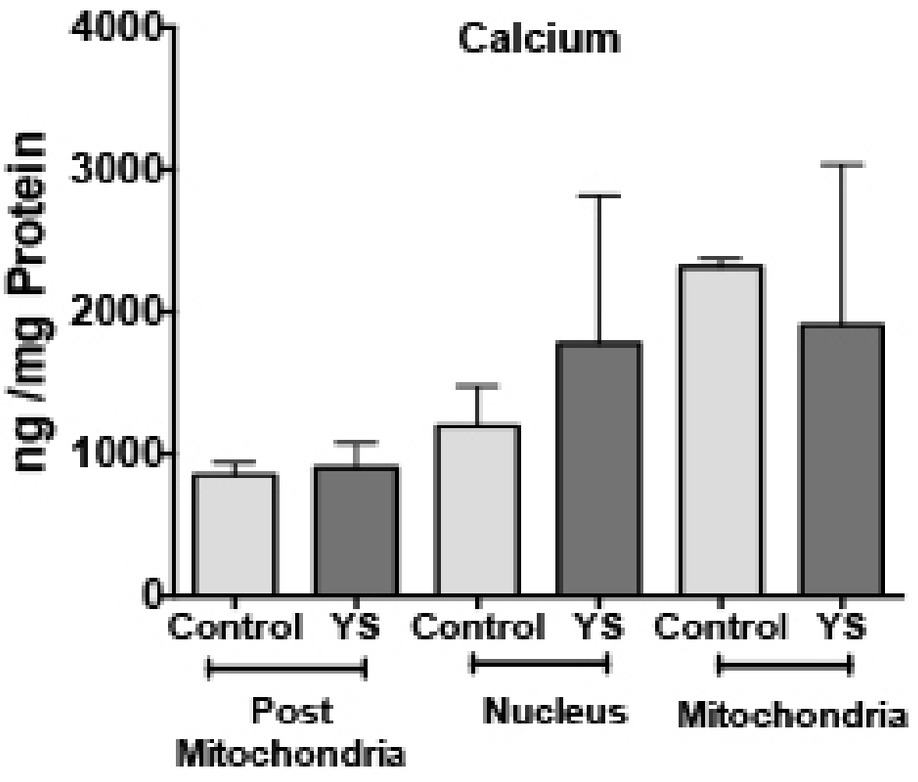
Calcium
ng /mg Protein
4000
3000
2000
1000
0
Control YS Control YS Control YS
Post Mitochondria
Nucleus
Mitochondria

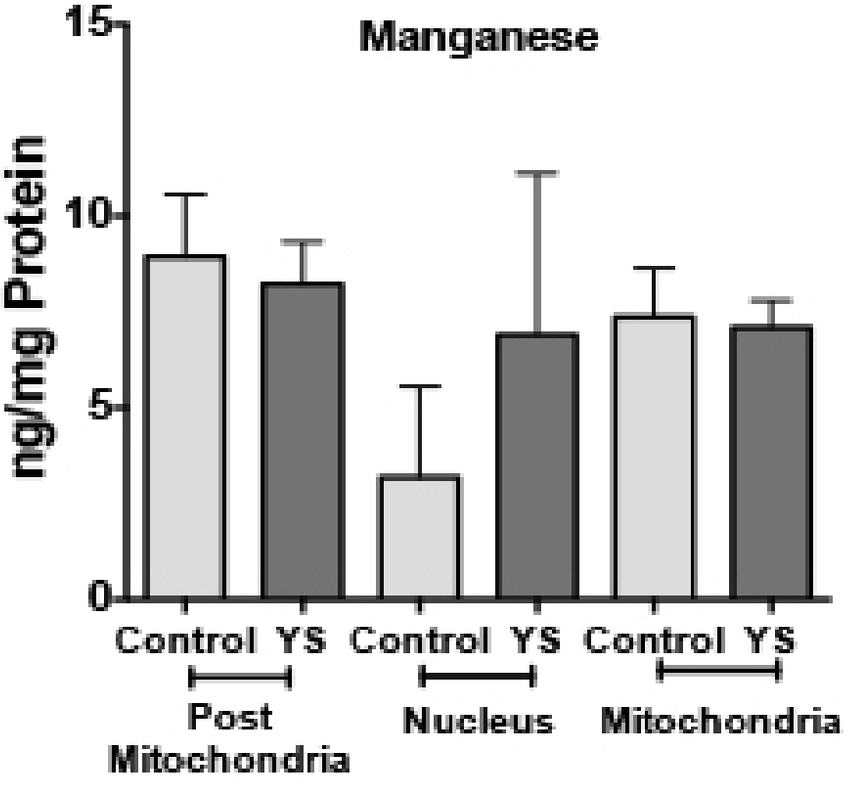
Manganese
ng/mg Protein
15
10
5
0
Control YS Control YS Control YS
Post Mitochondria
Nucleus
Mitochondria

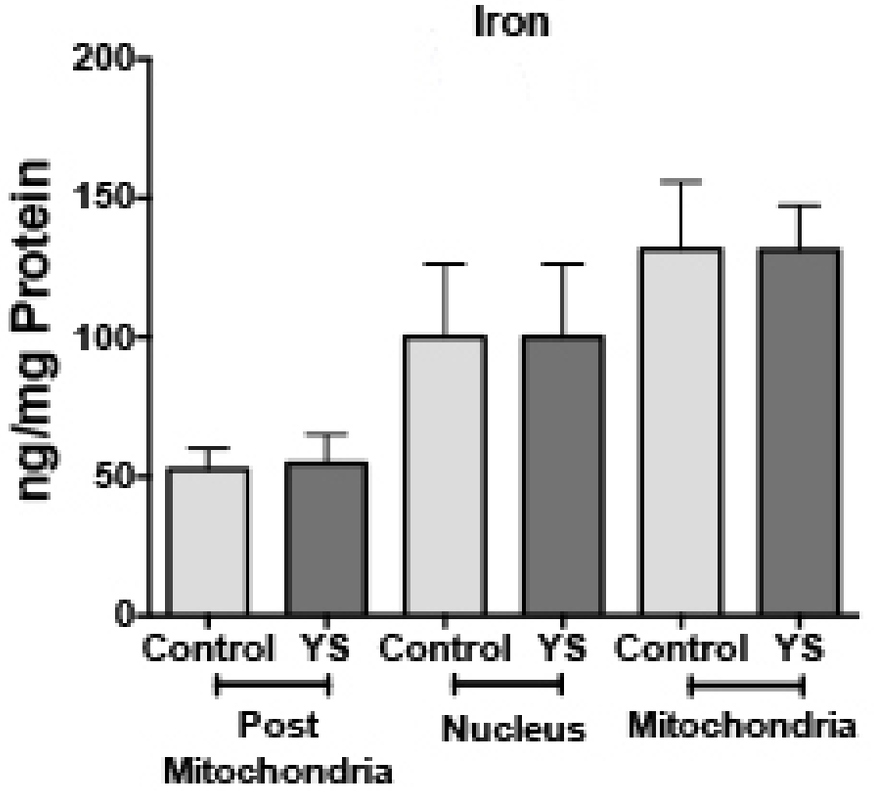
Iron
ng/mg Protein
200
150
100
50
0
Control YS Control YS Control YS
Post Mitochondria
Nucleus
Mitochondria

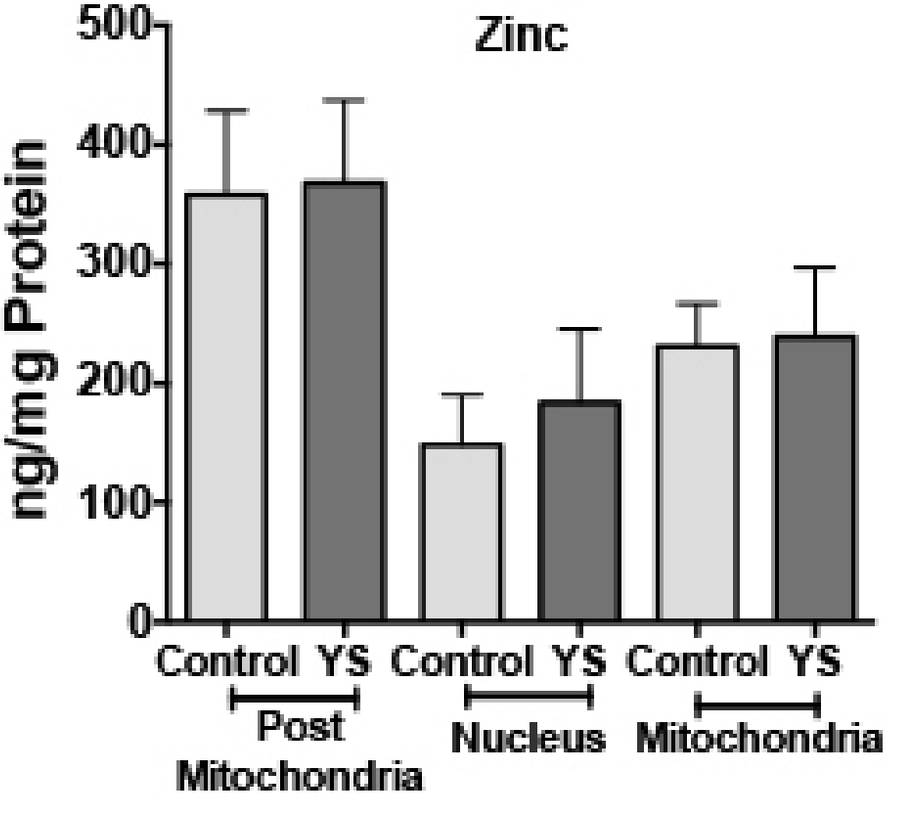
Zinc
ng/mg Protein
500
400
300
200
100
0
Control YS Control YS Control YS
Post Mitochondria
Nucleus
Mitochondria

Figure 3

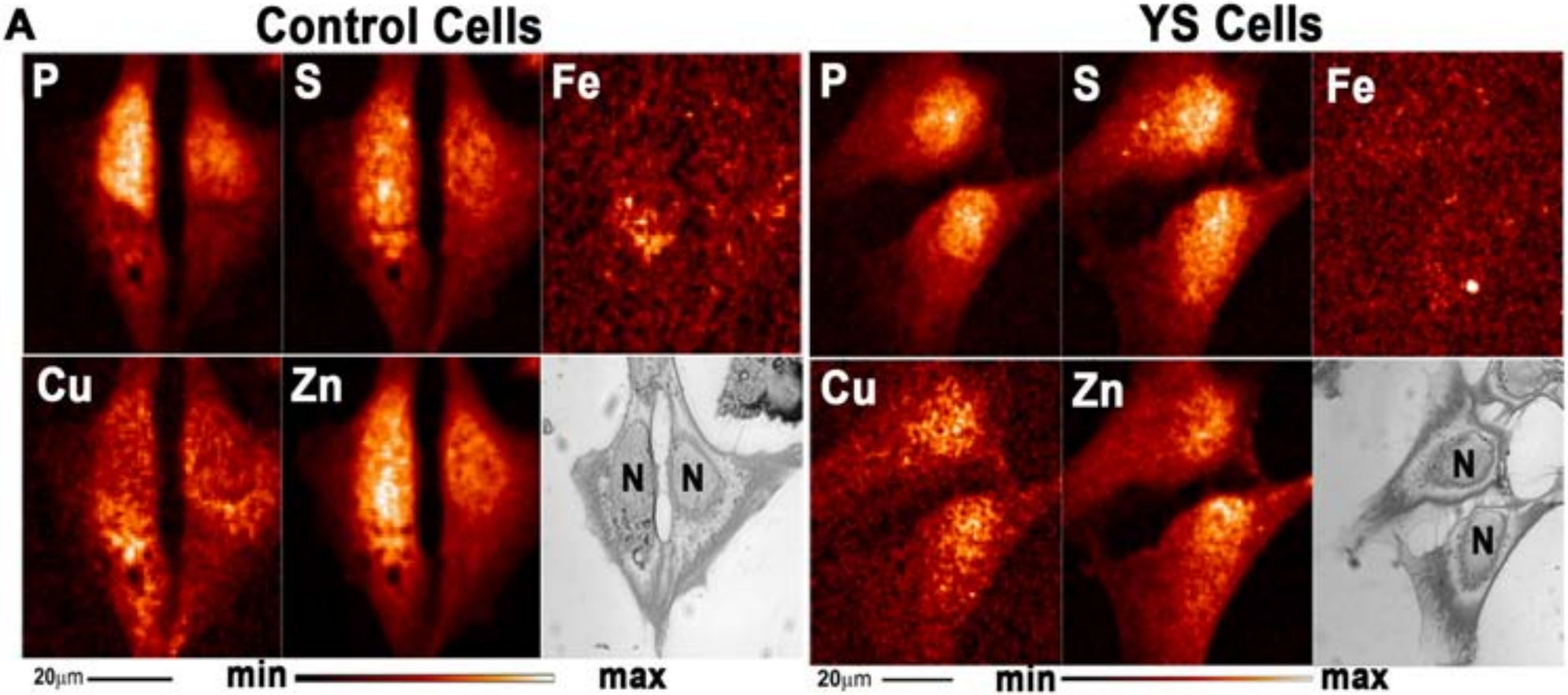
A
Control Cells
YS Cells
P
S
Fe
Cu
Zn
N
N
20μm
min
max
B
Relative mRNA Expression (Metallothionein1)
1.5
1.0
0.5
0.0
***
Control
YS
C
Relative Expression (mRNA)
10
8
6
4
2
0
MT1a
MT2a
Control
YS

Figure 4

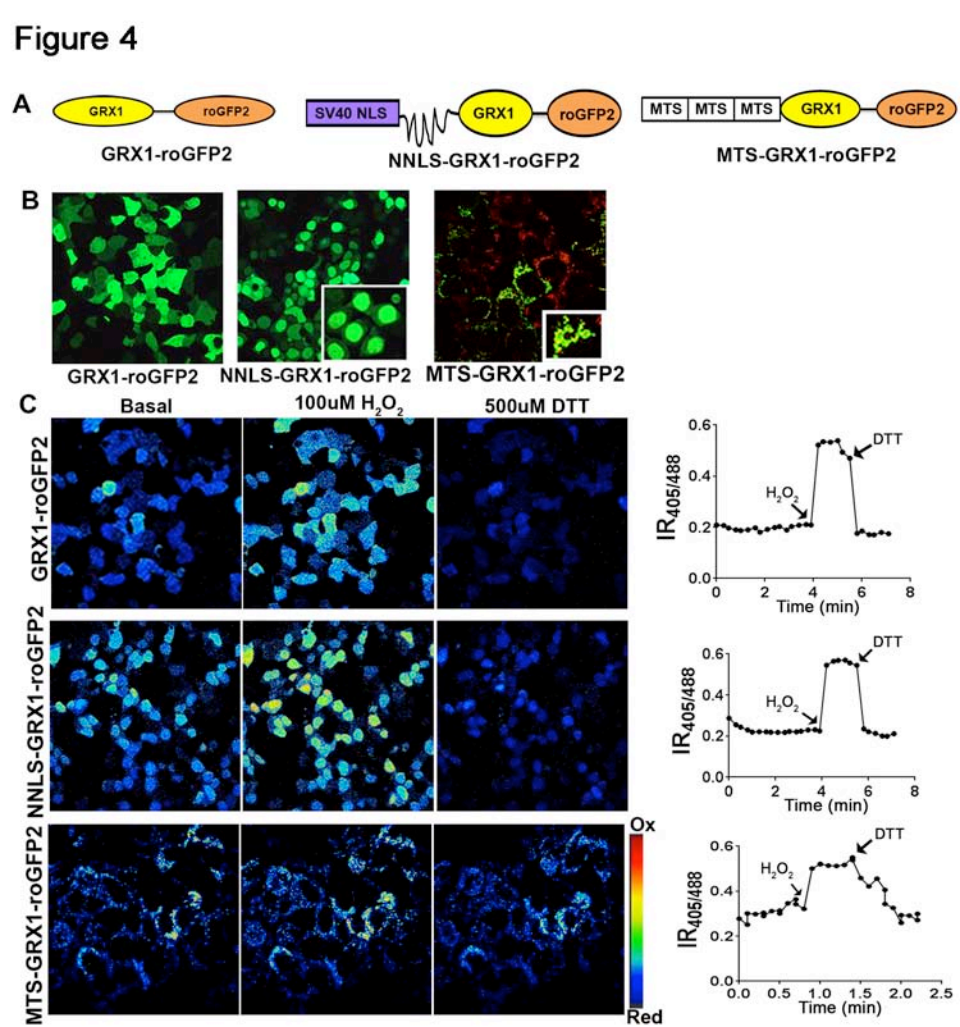
A
GRX1
roGFP2
GRX1-roGFP2
SV40 NLS
GRX1
roGFP2
NNLS-GRX1-roGFP2
MTS
MTS
MTS
GRX1
roGFP2
MTS-GRX1-roGFP2
B
GRX1-roGFP2
NNLS-GRX1-roGFP2
MTS-GRX1-roGFP2
C
Basal
100uM H2O2
500uM DTT
GRX1-roGFP2
NNLS-GRX1-roGFP2
MTS-GRX1-roGFP2
Ox
Red
IR405/488
H2O2
DTT
Time (min)

Figure 5

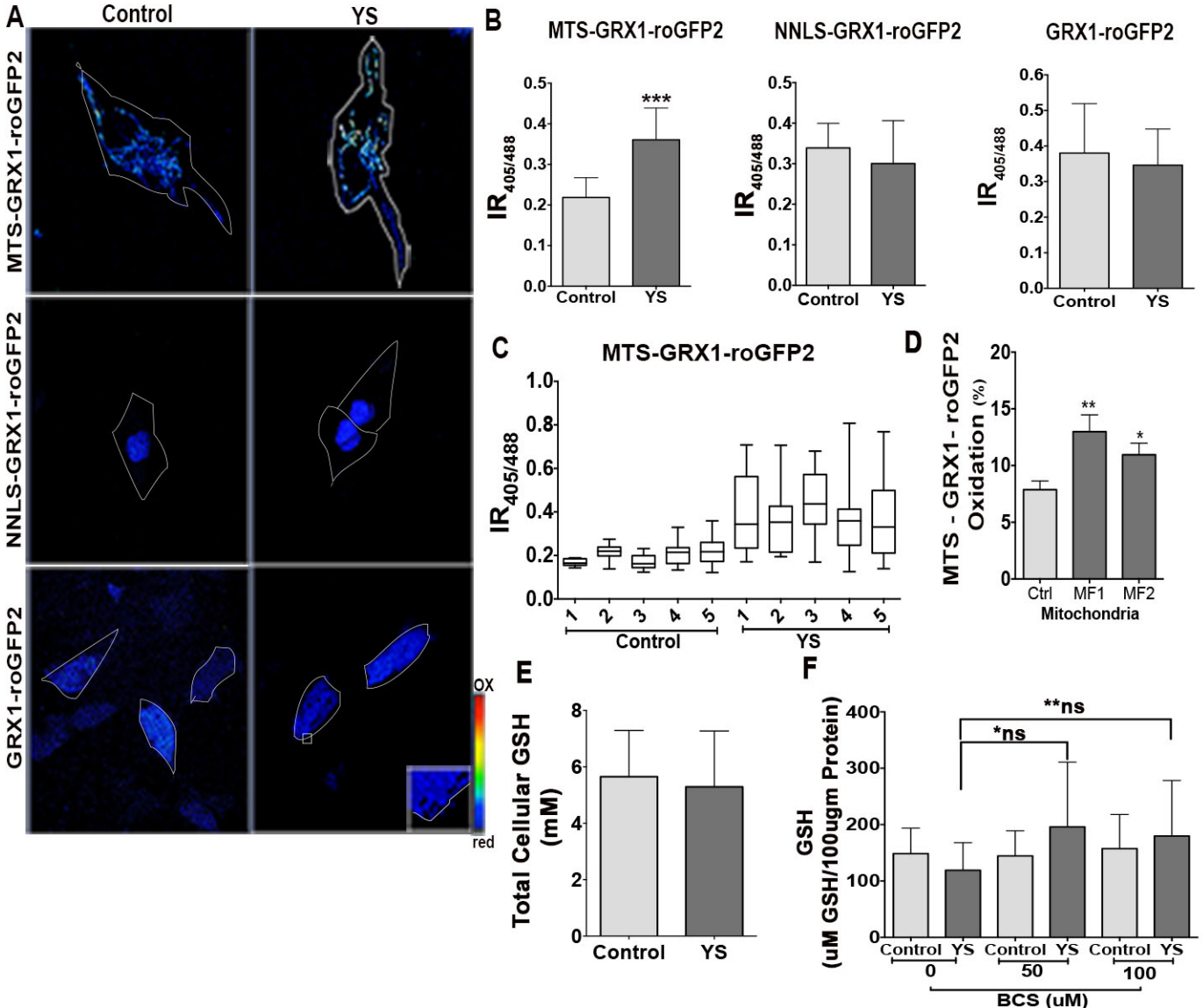
A
Control
YS
MTS-GRX1-roGFP2
NNLS-GRX1-roGFP2
GRX1-roGFP2
OX
red
B
MTS-GRX1-roGFP2
NNLS-GRX1-roGFP2
GRX1-roGFP2
IR405/488
***
Control
YS
C
MTS-GRX1-roGFP2
IR405/488
Control
YS
D
MTS - GRX1- roGFP2 Oxidation (%)
**
*
Ctrl
MF1
MF2
Mitochondria
E
Total Cellular GSH (mM)
Control
YS
F
GSH (uM GSH/100ugm Protein)
**ns
*ns
Control
YS
0
50
100
BCS (uM)

Figure 6

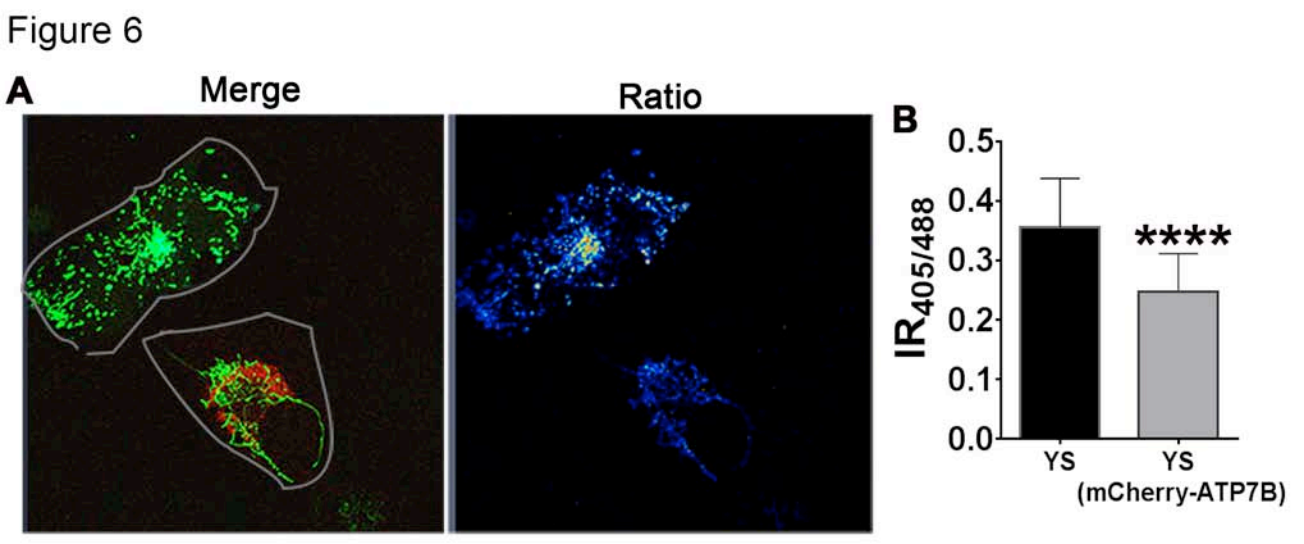

Figure 7

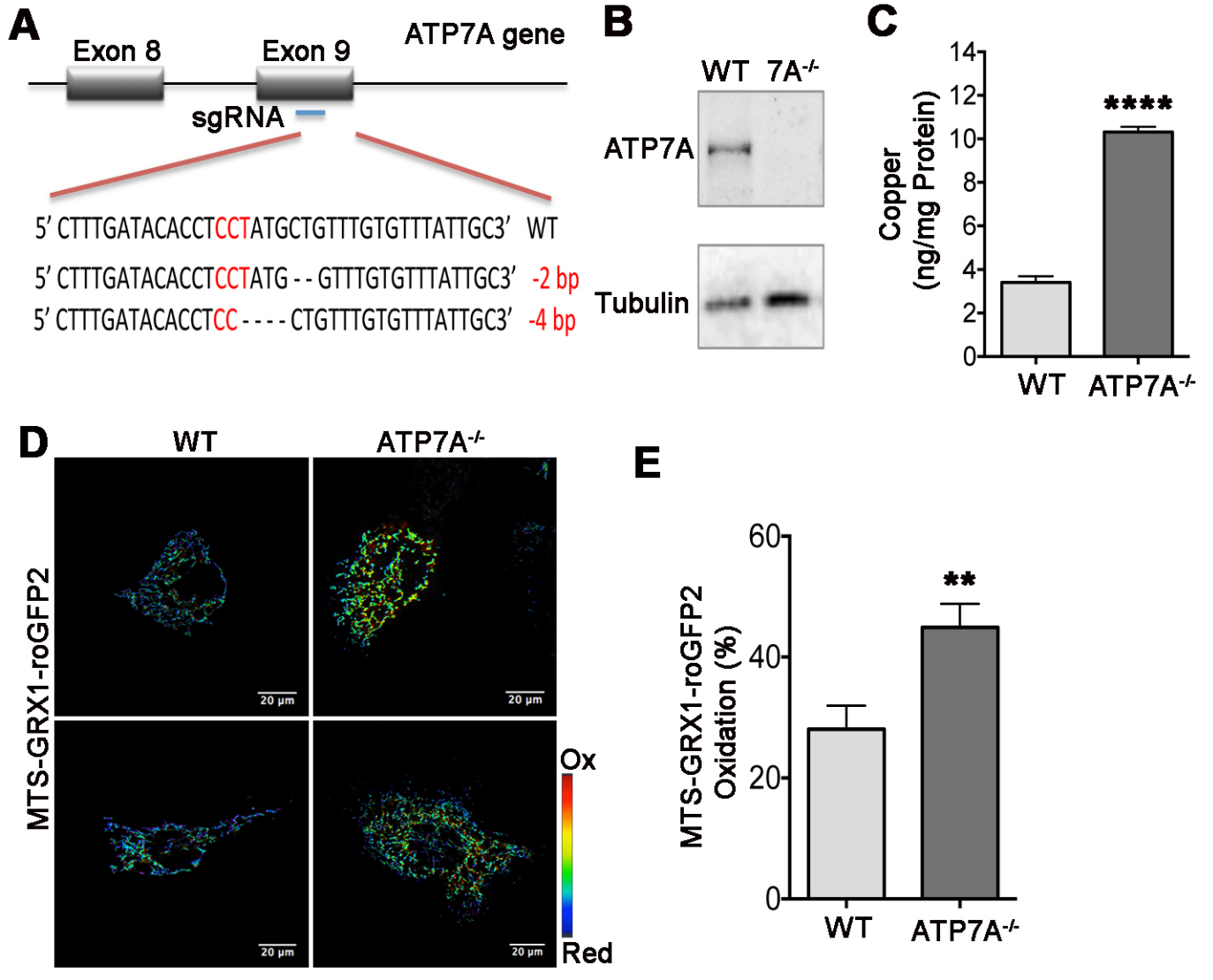
A
Exon 8
Exon 9
ATP7A gene
sgRNA
5′ CTTTGATACACCTCCTATGCTGTTTGTGTTTATTGC3′ WT
5′ CTTTGATACACCTCCTATG - - GTTTGTGTTTATTGC3′ -2 bp
5′ CTTTGATACACCTCC - - - - CTGTTTGTGTTTATTGC3′ -4 bp
B
WT 7A-/-
ATP7A
Tubulin
C
Copper (ng/mg Protein)
14
12
10
8
6
4
2
0
****
WT
ATP7A-/-
D
WT
ATP7A-/-
MTS-GRX1-roGFP2
20 µm
Ox
Red
E
MTS-GRX1-roGFP2 Oxidation (%)
60
40
20
0
**
WT
ATP7A-/-

Figure 8

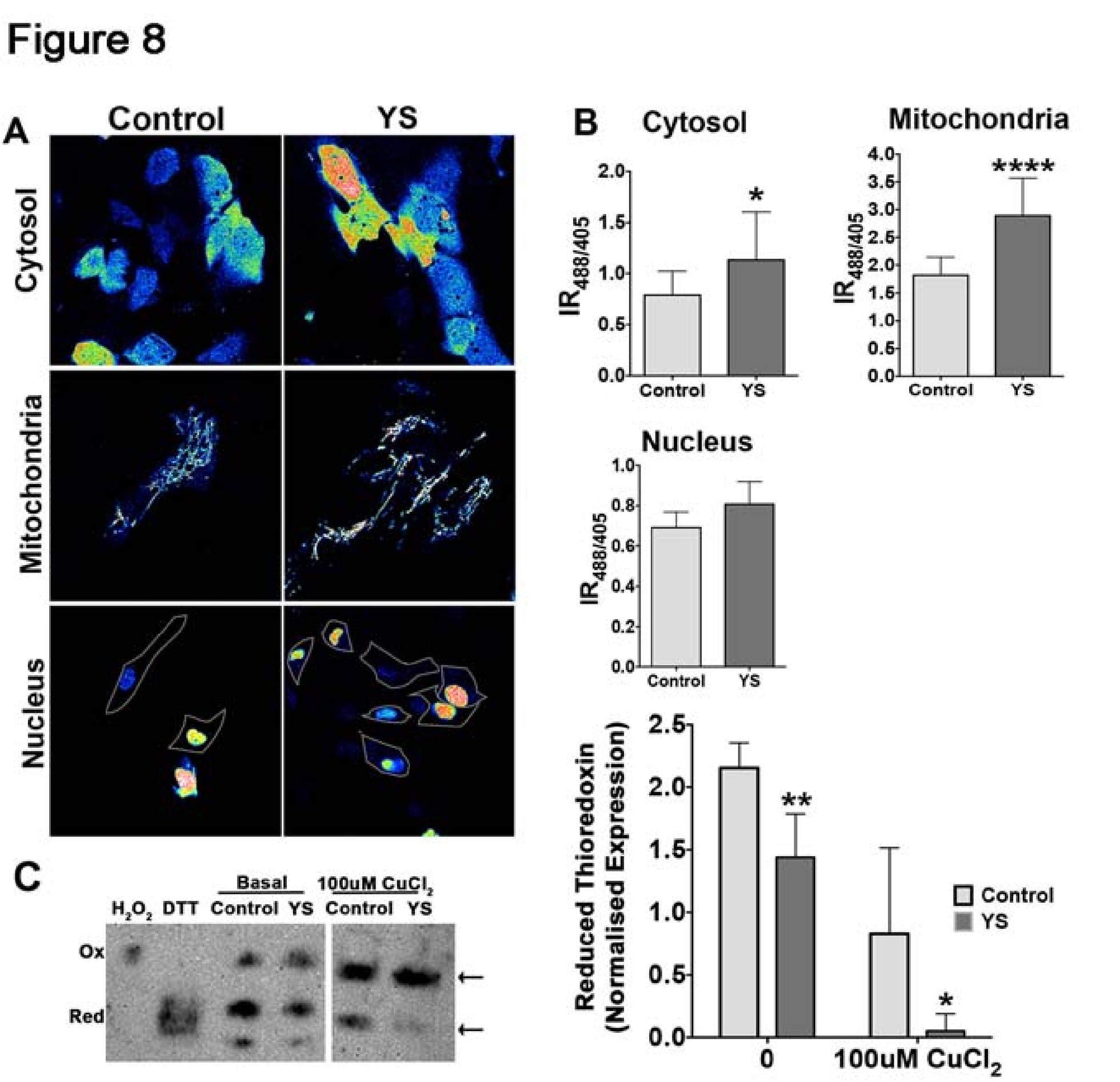
A
Control
YS
Cytosol
Mitochondria
Nucleus
B
Cytosol
Mitochondria
Nucleus
IR488/405
Control
YS
*
****
C
Basal
100uM CuCl2
H2O2
DTT
Control
YS
Control
YS
Ox
Red
Reduced Thioredoxin (Normalised Expression)
**
*
0
100uM CuCl2

Figure 9

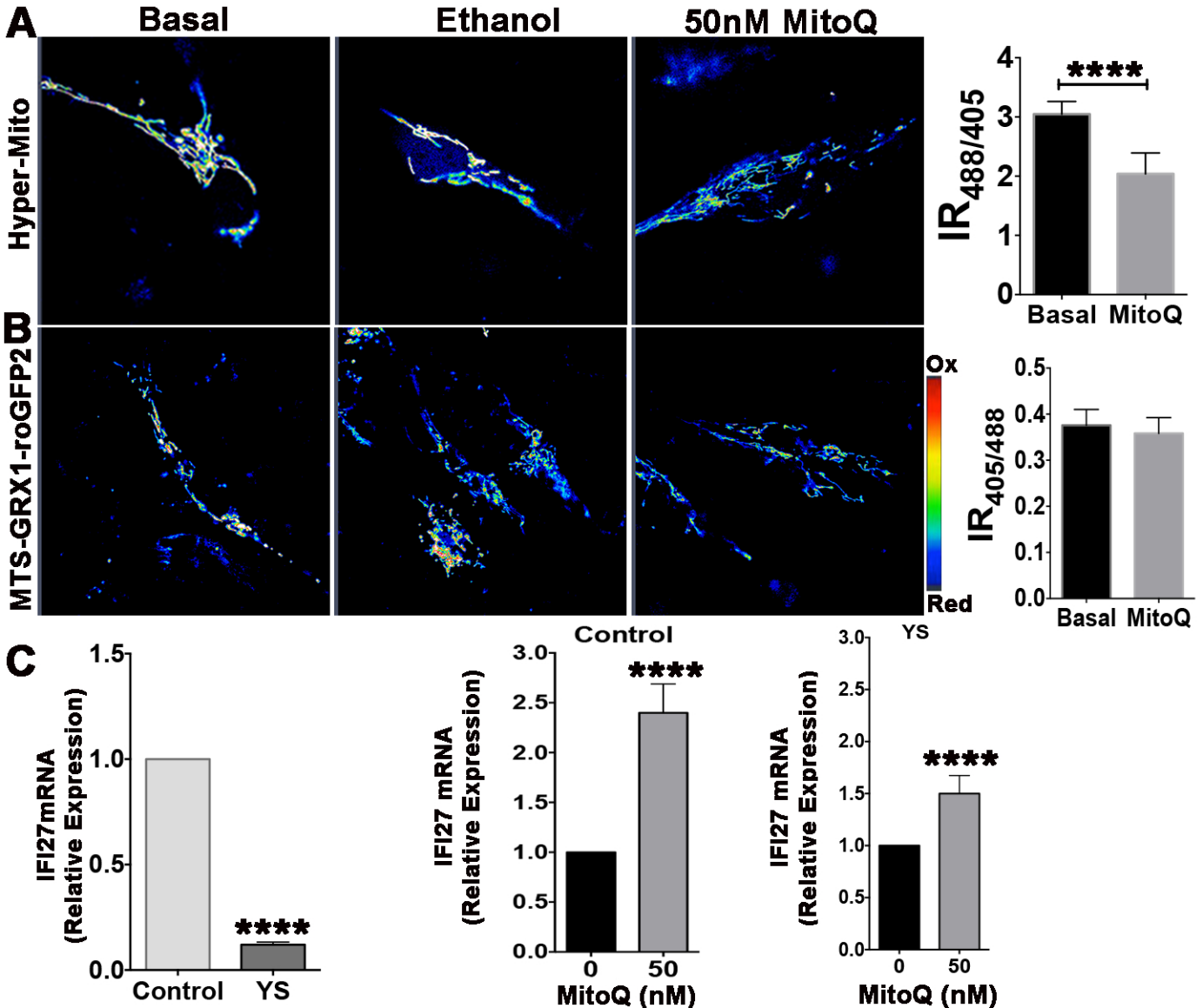
A
Basal
Ethanol
50nM MitoQ
Hyper-Mito
B
MTS-GRX1-roGFP2
Ox
Red
$IR_{488/405}$
****
Basal
MitoQ
$IR_{405/488}$
Basal
MitoQ
C
IFI27mRNA (Relative Expression)
****
Control
YS
IFI27 mRNA (Relative Expression)
Control
****
0
50
MitoQ (nM)
IFI27 mRNA (Relative Expression)
YS
****
0
50
MitoQ (nM)

Figure 10

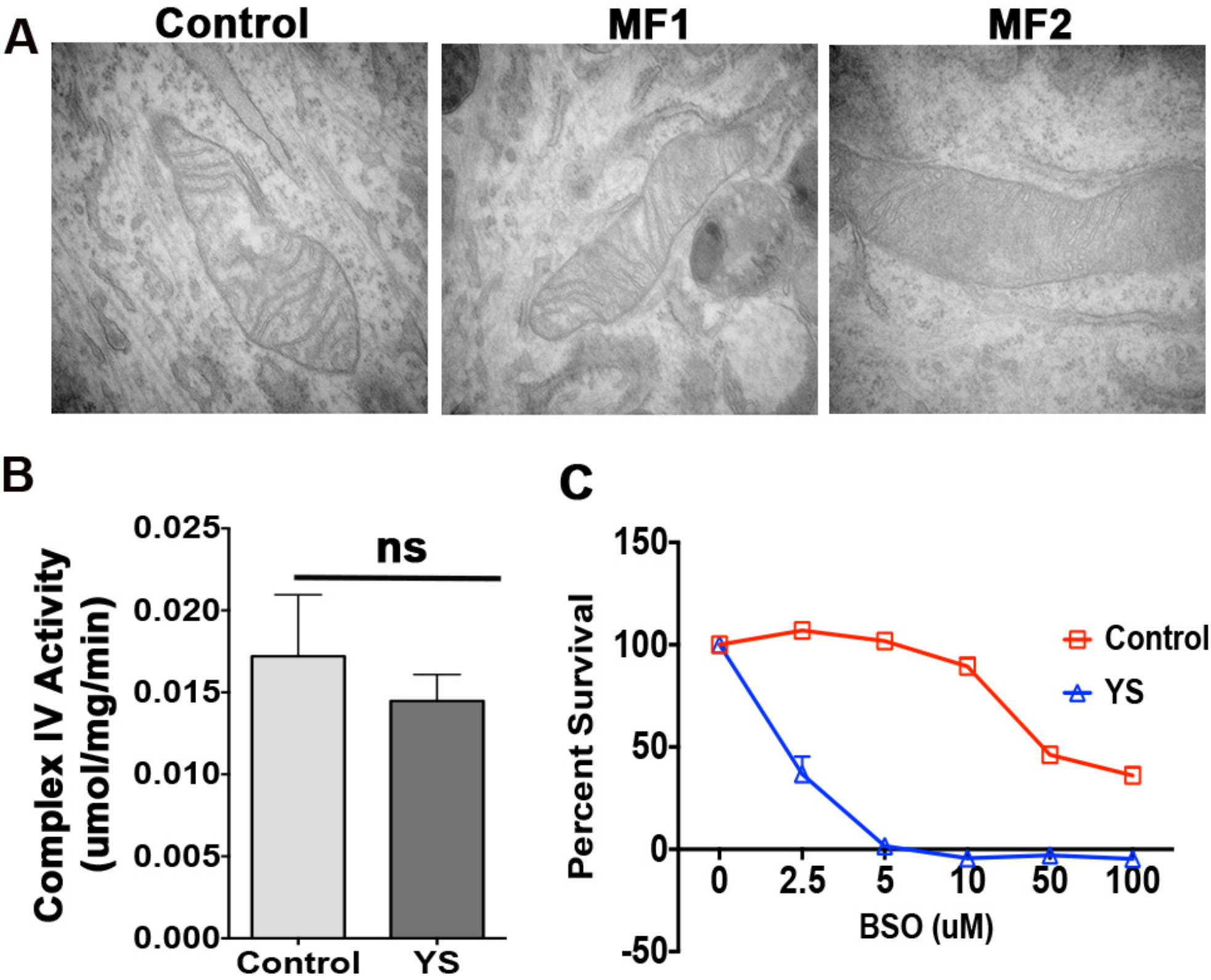
A
Control
MF1
MF2
B
Complex IV Activity (umol/mg/min)
0.025
0.020
0.015
0.010
0.005
0.000
ns
Control
YS
C
Percent Survival
150
100
50
0
-50
0
2.5
5
10
50
100
BSO (uM)
Control
YS

Activity of Menkes Disease Protein ATP7A is Essential for Redox Balance in Mitochondria

Ashima Bhattacharjee, Haojun Yang, Megan Duffy, Emily Robinson, Arianrhod Conrad-Antoville, Ya-Wen Lu, Tony Capps, Lelita T. Braiterman, Michael J. Wolfgang, Michael Patrick Murphy, Ling Yi, Stephen G. Kaler, Svetlana Lutsenko and Martina Ralle

J. Biol. Chem. published online May 16, 2016
